

1 **A Geochemical Record of Late-Holocene Hurricane Events from the**
2 **Florida Everglades**

3
4 **Qiang Yao¹, Kam-biu Liu¹, Erika Rodrigues², Thomas Bianchette³, Alejandro**
5 **Antonio Aragón-Moreno^{1*}, Zhenqing Zhang^{4*}**

6
7 ¹Department of Oceanography and Coastal Sciences, College of the Coast and
8 Environment, Louisiana State University, Baton Rouge, LA 70803

9
10 ²Laboratory of Coastal Dynamics, Graduate Program of Geology and Geochemistry,
11 Federal University of Pará, Brazil Federal University of Pará. Rua Augusto Corrêa, 01
12 - Guamá. CEP 66075-110, Belém (PA), Brazil.

13
14 ³Department of Natural Sciences, College of Arts, Sciences, and Letters, University
15 of Michigan-Dearborn, Dearborn, MI 48128

16
17 ⁴School of Geographic and Environmental Sciences, Tianjin Normal University,
18 Tianjin, China

19
20
21 *Corresponding authors:

22 Alejandro Antonio Aragón-Moreno, aragonmoreno1@lsu.edu

23 Zhenqing Zhang, zhangzq@neigae.ac.cn

24
25
26 **Key Points:**

- 27
- 28 • This study demonstrates the use of XRF analysis in detecting major hurricane
29 events in sand-limited coastal systems.
 - 30 • Five active hurricane periods were identified at ~3400-3000, ~2200-1500,
31 ~1000-800, ~600-300, and ~150 cal yr BP to present.
 - 32 • This study suggests that intense hurricane activities in the western Atlantic
33 Basin was modulated by ITCZ, ENSO, and NAO activities.
- 34
35
36

This is the author manuscript accepted for publication and has undergone full peer review but has not been through the copyediting, typesetting, pagination and proofreading process, which may lead to differences between this version and the Version of Record. Please cite this article as doi: [10.1029/2019WR026857](https://doi.org/10.1029/2019WR026857)

37 **Abstract**

38 A 5.25 m sediment core SRM-1 and 45 surface samples from mangrove forests at the
39 Shark River Estuary in the Everglades National Park, Florida, was examined by using
40 X-ray fluorescence and carbon isotopic analyses to study the history of intense
41 hurricane landfall during the Late-Holocene. Significance testing of the surface
42 samples in relation to storm deposits from Hurricane Wilma suggests that elemental
43 concentration of Sr and Cl and the ratio of Cl/Br are the most sensitive indicators for
44 major hurricane events in our study area. The geochemical datasets of core SRM-1
45 identified five active periods of intense hurricane activities during the last 3500 years
46 at ~3400-3000, ~2200-1500, ~1000-800, ~600-300, and ~150 cal yr BP to present.
47 This is the longest paleohurricane record to date from South Florida. Our results are
48 consistent with the view that intense hurricane activities in South Florida were
49 modulated by ITCZ movements, ENSO activities, and NAO strength. This study
50 contributes to the methodological advancement in paleotempestological studies by
51 demonstrating that geochemical signals, particularly signals of saltwater intrusions,
52 can be preserved in the sediment profiles on millennial time-scale and measured by
53 XRF techniques, thereby enabling more storm records to be produced from otherwise
54 suboptimal sand-limited coastal systems such as the Florida Everglades. More work
55 needs to be done to explore the use of geochemical and stable isotopic analyses in
56 detecting storm signals from sand-limited coastal environments.

57

58 **Plain Language Summary**

59 This study uses geochemical analyses to detect intense hurricanes that made landfall
60 near the southwest coast of the Florida Everglades from sediment profiles. The
61 geochemical datasets identified five active periods of intense hurricane activities
62 during the last 3500 years at ~3400-3000, ~2200-1500, ~1000-800, ~600-300, and
63 ~150 years ago. Results from this study agree with previous studies that intense
64 hurricane activities in the western Atlantic Basin were controlled by the position of
65 ITCZ, ENSO activities, and NAO strength.

66

67

68 1. Introduction

69 Tropical cyclones, including hurricanes, are among the most devastating weather
70 phenomena. During the last two decades, tropical cyclones have caused over 200,000
71 fatalities and affected the lives of over 700 million people worldwide (WHO, 2020).
72 In the Atlantic and the Eastern North Pacific Basin, hurricanes devastate the lives of
73 tens of millions of people living in the coastal zones across the United States and
74 Central America every year. Among the hurricane-prone regions in the United States,
75 South Florida is particularly vulnerable to intense hurricane landfall because it can be
76 impacted by storms coming from both the Atlantic and Gulf of Mexico (GOM)
77 regions. According to the observational record between 1842 CE and 2019 CE, South
78 Florida was struck by 36 hurricanes (NOAA, 2019). The average return interval of
79 hurricane landfall is ~ 5 years. Such unique geographical setting makes South Florida
80 an ideal location to study the behavior of North Atlantic hurricanes. In particular,
81 along the coastlines of the Everglades National Park (ENP), approximately 144,000
82 ha of protected wetlands occupy the coastal zones from Naples to Florida Bay (Lodge,
83 2016; Simard et al., 2006). The sediment profiles of these undisturbed coastal
84 wetlands started to accumulate since over 5000 years ago (Yao et al., 2015; Yao &
85 Liu, 2017), providing pristine archives to study the long-term pattern of hurricane
86 landfall since the mid-Holocene, far beyond the instrumental record.

87
88 Paleotempestology, a relatively young field in the geosciences (Liu, 2004, 2013; Liu
89 & Fearn, 1993, 2000), provides the best means to reconstruct the occurrence of
90 paleohurricane events from the proxy record and predict the future variabilities in
91 hurricane frequency. However, paleohurricane proxy records are remarkably rare
92 from the densely populated South Florida coasts (Ercolani et al., 2015), and few well-
93 dated storm records longer than 1000 years in length exist in the region (Glaser et al.,
94 2013; Van Soelen et al., 2012). The dearth of paleohurricane record is partially due to
95 the sand-limited coastal wetland environment in South Florida, which has posed a
96 challenge to the application of conventional methodology in paleotempestology.

97
98 Traditionally, the identification of storm surge deposits has been achieved by using a
99 combination of physical indicators (e.g., % water, % organics, % carbonates, and
100 grain size). In particular, the most useful proxy for paleotempestological studies to
101 date has been overwash sand layers preserved in sediment cores retrieved from
102 backbarrier lakes and marshes along the coastal zones (e.g., Brandon et al., 2013;
103 Donnelly et al., 2001; Donnelly et al., 2001; Donnelly & Woodruff, 2007; Gao et al.,
104 2019; Lane et al., 2011; Liu, 2004, 2013; Mann et al., 2009; Wallace et al., 2014;
105 Wallace & Anderson, 2010; Woodruff et al., 2008; Yao et al., 2018; Bregy et al.,
106 2018; Zhou et al., 2017, 2019). However, the usefulness of this sedimentological
107 proxy may be problematic in a sand-limited or peat-dominated coastal environment,
108 such as the Florida Everglades (Lodge, 2016). Previous studies have indicated that
109 sediment profiles retrieved from the coastal Everglades consist of primarily peat
110 deposits (>50% organic matters) with very little clastic materials (Yao et al., 2015;
111 Yao & Liu, 2017). Accordingly, the use of geochemical proxies, such as X-ray
112 fluorescence (XRF) and isotopic analyses, should be explored.

113
114 XRF analysis is a non-invasive geochemical analytical technique that can be used to
115 quantify many of the common chemical elements in coastal sediments. This technique
116 has been successfully used to detect marine-originated sediments in coastal
117 environments and to identify some potential indicators (e.g., Ca, Sr, Cl, and Cl/Br) of

118 storm or tsunami deposits in sediment cores (Bianchette et al., 2016; McCloskey et
119 al., 2015; McCloskey et al., 2018; McCloskey & Liu, 2012 a&b, 2013; Naquin et al.,
120 2014; Ramírez-Herrera et al., 2012; Yao et al., 2019). Given the sedimentological
121 condition of South Florida (Yao & Liu, 2018) and site-specificity of storm
122 sedimentation processes (Williams & Liu, 2019; Yao et al., 2019), identifying the
123 sensitive chemical indicators for storm deposits is the key to accurately detecting
124 paleohurricane events in sediment profiles from the region. However, the existing
125 datasets lack robust significance testing of the XRF parameters in relation to a modern
126 hurricane.

127
128 In addition, the use of carbon isotopic analysis in paleotempestological studies should
129 also be explored. Because various sources of carbon show distinct differences in
130 carbon isotopic ratios ($\delta^{13}\text{C}$) and organic carbon to total nitrogen ratios (C/N),
131 variations in $\delta^{13}\text{C}$ and C/N have been used to describe the origin of organic materials
132 preserved in coastal environments (Chmura & Aharon, 1995; Lamb et al., 2006;
133 Lambert et al., 2008). In a peat-dominated coastal environment such as the
134 Everglades, these isotopic indicators are expected to be more sensitive in detecting the
135 marine incursion events in regard to the conventional sedimentological proxy used in
136 previous paleotempestological studies. However, among long-term hurricane records
137 from Florida, few attempts have been made in using carbon isotopic analysis to detect
138 paleohurricane events in sediment profiles (Das et al., 2013; Lambert et al., 2008).

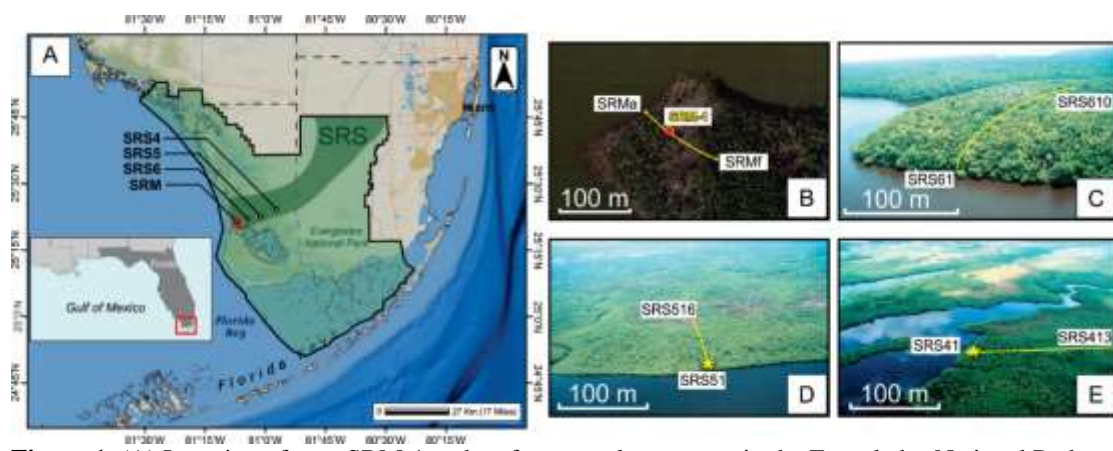
139
140 In this paper, we aim to fill the above-mentioned data gaps and explore the use of
141 XRF and isotope analyses to identify paleohurricane events in Southwest Florida
142 based on 45 surface samples and a 5.25 m sediment core (SRM-1) retrieved in the
143 ENP. The surface samples were taken along a 20 km transect with distinct marine-to-
144 terrestrial gradient and core SRM-1 contains over 5700 years of sedimentary history
145 including ~10 cm of distinctive storm deposit attributable to Hurricane Wilma (2005)
146 at the top of the core. The main objectives of this study are to (1) reveal the hurricane
147 indicators in a peat-dominated coastal environment by characterize the chemical
148 signature of Hurricane Wilma deposits; (2) identify evidence of intense
149 paleohurricane events during the Late-Holocene in the sedimentary record; and (3)
150 reconstruct the history of paleohurricane strikes in the Shark River Slough in the
151 context of Late-Holocene environmental changes in the Florida Coastal Everglades.

152 153 **2. Materials and Methods**

154 **2.1 Study Area**

155 The coring site for SRM-1 (25°21'10" N, 81°6'52" W) is located on the edge of
156 Ponce de Leon Bay, at the coastal junction where the Shark River Slough, the largest
157 slow-moving flow of freshwater in the Florida Everglades, meets the saltwater of the
158 GOM (Figure. 1). Historically, water overflowing Lake Okeechobee and associated
159 rainfall results in a southward sheet flow along a gentle slope of ~3 cm/km down
160 Shark River Slough into the GOM (Lodge, 2016). The 45 surface samples were taken
161 from 4 main study areas (SRM, SRS-6, SRS-5, and SRS-4) along the Shark River
162 Slough (Figure. 1). Site SRM is situated at the mouth of the Shark River Slough and
163 sites SRS-6, SRS-5, and SRS-4 are part of the Florida Coastal Everglades Long-term
164 Ecological Research (LTER) sites situated at approximately 4 km, 8 km, and 20 km
165 upstream from SRM, respectively. The 4 study areas are located along a distinct
166 marine-to-terrestrial transect. Accordingly, the overall salinity, though fluctuating
167 overtime due to tidal and seasonal changes, decreases significantly upstream from

168 SRM (>30 ppt) to SRS-6 (27 ± 2.6 ppt), SRS-5 (20.8 ± 3.1 ppt), and SRS-4 (4.6 ± 1.1
 169 ppt). The GPS and salinity data of all the surface samples can be found in online
 170 supplementary content (Table. S1).
 171



172
 173 **Figure 1.** (A) Location of core SRM-1 and surface sample transects in the Everglades National Park,
 174 South Florida. (B) The yellow line indicates the transect where surface samples SRMA to SRMf
 175 were taken. The red dot points to core SRM-1. (C) Transect SRS6 where surface samples SRS61 to SRS610
 176 were taken (D) Transect SRS5 where surface samples SRS51 to SRS516 were taken. (E) Transect
 177 SRS4 where surface samples SRS41 to SRS413 were taken. See Table. S1 for more details about the
 178 surface samples.
 179

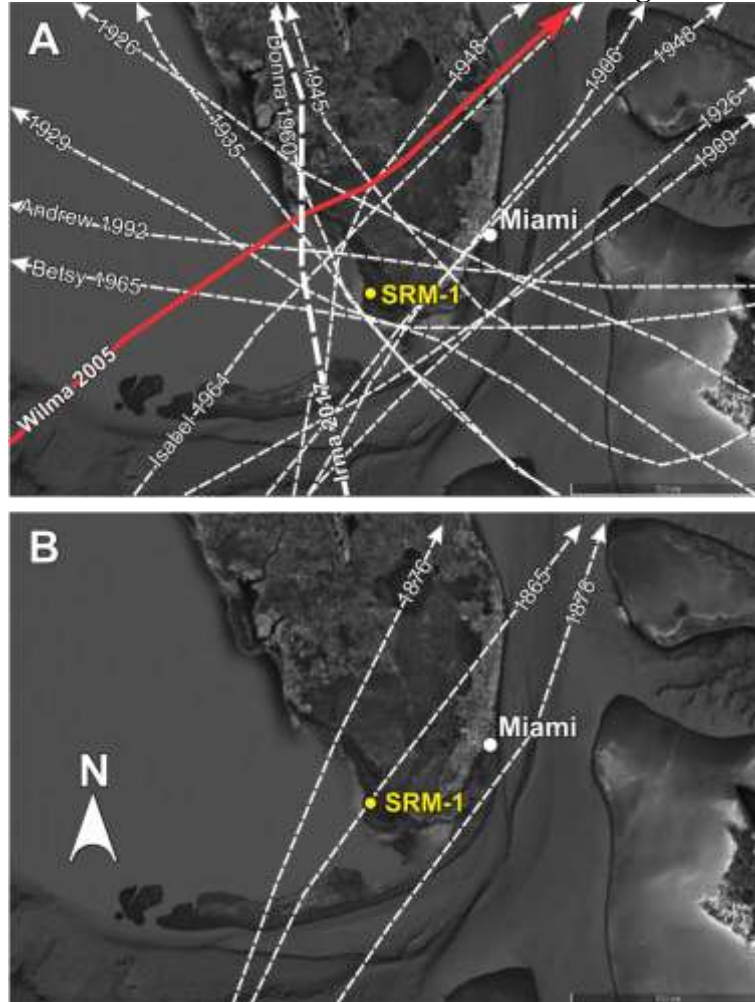
180 Recent studies from the Shark River Slough indicate that our study areas were
 181 situated on a dry and upland environment before the mid-Holocene (Yao & Liu,
 182 2017). As a result of the rapid sea level rise and increasing water table in South
 183 Florida, freshwater marsh started to appear at the Shark River Mouth (SRM) during
 184 the mid-Holocene (Yao et al., 2015). As marine transgression continued between
 185 5700 and 3500 cal yr BP, brackish marsh started to appear at the SRM area and
 186 freshwater marsh progressively expanded inland and upstream from site SRM to SRS-
 187 4 along the Shark River Slough (Yao & Liu, 2017, 2018). At ~ 3500 cal yr BP, due to
 188 the establishment of mangrove forests and decelerating sea level rise (<0.4 mm/yr
 189 after ~3500 cal yr BP), marine transgression has stabilized at coastlines along South
 190 Florida (Parkinson, 1989; Scholl et al., 1969; Wanless et al., 1994). During the next
 191 2000 years, mangroves continue to expand and a dense *Rhizophora mangle*-
 192 dominated mangrove forest was formed at the mouth of the Shark River Slough at
 193 ~1150 cal yr BP, when the shoreline reached its modern position at the Shark River
 194 Estuary (Yao et al., 2015). Pollen and sedimentary record shows that since ~1150 cal
 195 yr BP, site SRM has been sitting on a fringing mangrove forest, where *Laguncularia*
 196 *racemosa* (white mangrove) and *Rhizophora mangle* (red mangrove) are co-dominant
 197 species, and *Avicennia germinans* (black mangrove) is also present. The hydroperiod
 198 in the study site is influenced mainly by tidal cycles. Accordingly, the mangrove
 199 forests at the study area are inundated by tides 90% of the year, with an average tidal
 200 range of 0.5 m (Yao et al., 2015), and soil pore-water salinity is ~30 ppt (Yao & Liu,
 201 2017).
 202

203 Studies have shown that hurricanes play an important role in regulating the structure
 204 of mangrove forests at the mouth of Shark River Slough (Chen & Twilley, 1999a,
 205 1999b; Smoak et al., 2013). Mineral and sediment inputs during storm events from the
 206 GOM, rather than inputs from upland, enhance nutrient concentrations in the coastal
 207 area, causing higher biomass and tree height in the fringing mangrove forest (SRM

208 and SRS-6) in contrast to upstream sites (SRS 5 and SRS-4) of this estuary and other
 209 regions of southeastern Florida (Castañeda-Moya et al., 2010, 2013, 2020). Hence, the
 210 average height of mangroves trees at site SRM are among the highest in southwestern
 211 Florida (>25 m) (Simard et al., 2006).

212
 213

2.2 Historical Hurricanes and their Meteorological Characteristics



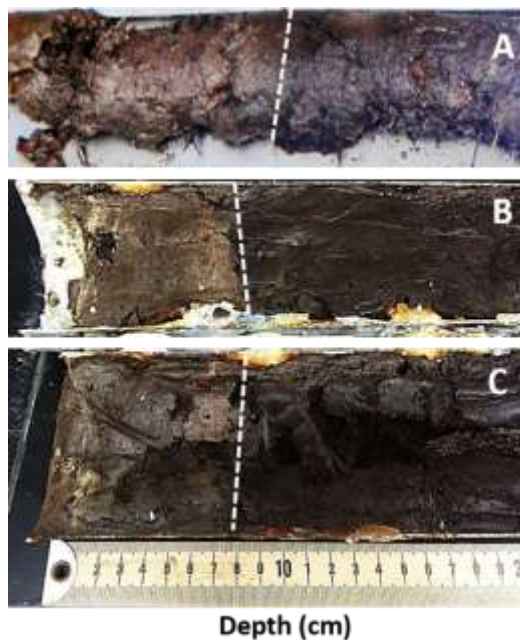
214
 215 **Figure 2.** Aerial image of hurricane landfalls in South Florida near our study site (within 100 km). A)
 216 Fifteen intense hurricanes (category 3-5 according to the Saffir-Simpson scale) from AD 1900 to 2019.
 217 B) All recorded hurricanes before AD 1900. Arrows indicate direction of the hurricane. (Figures
 218 modified from National Oceanic and Atmospheric Administration, Historical Hurricane Tracks
 219 website: <https://coast.noaa.gov/hurricanes/>)
 220

221 Instrumental record show that 3 hurricanes struck near our study area (within 100 km
 222 of core SRM-1) during the 19th century (NOAA, 2019). From 1901 to 2019 AD, 15
 223 intense hurricanes (category 3-5 according to the Saffir-Simpson scale) have made
 224 landfall near our study area (within 100 km), an average return interval of ~8 years
 225 (NOAA, 2019) (Figure. 2). During the 20th century, prior to the retrieval of core
 226 SRM-1 (May 2010), two category 5 storms, the Labor Day Hurricane and Hurricane
 227 Andrew, directly struck South Florida in 1935 and 1992 (Elsner & Kara, 1999). The
 228 Labor Day Hurricane was the first recorded category 5 hurricane to hit the United
 229 States. It crossed the middle Florida Keys, then moved northward parallel to the west
 230 Florida coastlines and made landfall near Cedar Key, approximately 460 km north of
 231 our study site (Smith et al., 2009). There are no estimates of storm surge and damage
 232 at our study area from this storm. Andrew made landfall on the southeast coast of the

233 Florida peninsula as a category 5 hurricane and exited into the GOM at ~30 km north
234 to our study site as a category 4 hurricane (Landsea et al., 2004). Although Andrew's
235 track was very close to our study area, it had a compact eye of ~15 km in radius
236 (Mayfield et al., 1994). The storm surge deposited sediment along a 13 km length of
237 coast from Highland Beach to Shark Point (Risi et al., 1995), just a few kilometers
238 north of our study site.

239
240 Hurricane Wilma was the most recent intense hurricane that made landfall near our
241 study area prior to the retrieval of core SRM-1 (May 2010). Compared with Andrew,
242 the track of Wilma was farther away from our study site (Figure. 2). It approached
243 South Florida from the southwest and made landfall as a category 3 hurricane on
244 October 24, 2005 near Everglades City, ~60 km north of our study site (Smith et al.,
245 2009). However, Wilma had an extremely large eye (a radius of ~50 km) at landfall,
246 with the northern eyewall passing south of Naples and the southern eyewall passing
247 approximately 10 km south of our study site (Zhang et al., 2008). It deposited up to 10
248 cm of sediment as far as 10 km inland from the GOM along a 70 km stretch of
249 coastline from Lostmans River to Flamingo (Castañeda-Moya et al., 2010; Smith et
250 al., 2009). When the storm passed our study area, the wind speed was 46 m/s and the
251 storm surge was 3 - 4 m (Castañeda-Moya et al., 2010). Hence, Wilma deposited
252 approximately 10 cm of marine sediments on top of the mangrove forest at site SRM
253 and SRS-6 (Figure. 3) (Castañeda-Moya et al., 2010; Smoak et al., 2013). As the
254 storm surge weakened toward the upstream areas of the Shark River Slough, storm
255 deposits of Hurricane Wilma gradually faded at site SRS-5 and were absent at site
256 SRS-4 (Castañeda-Moya et al., 2010; Yao & Liu, 2017). Strong winds and storm
257 surge from Wilma caused significant damages including defoliation, tree snapping,
258 and uprooting to approximately 1,250 ha of mangrove forest along the west coast of
259 the ENP, resulting in 90% mortality of trees with diameters at breast height greater
260 than 2.5 cm (Smith et al., 2009; Whelan et al., 2009).

261



262

263 **Figure 3.** Uppermost sedimentary unit of core SRM-1 (A), aluminum push core 1 (B), and aluminum
264 push core 2 (C). Eight to ten centimeters of storm deposits (above the white dash line) from Hurricane
265 Wilma are found at the top of all cores overlying the peat sediments.

266

267 The sensitivity of a study site to register evidence of hurricane strikes is affected by
268 several geomorphological and meteorological factors such as storm intensity, storm
269 surge height, site-to-sea distance, and direction of the landfalling storm (Liu, 2004,
270 2007; Liu & Fearn, 1993, 2000). It is important to note that in the northern
271 hemisphere, the peak storm surge occurs along the forward-right quadrant of the
272 landfalling hurricane (Liu, 2004, 2007). Therefore, storm surge heights are greater on
273 the right side of the landfalling hurricane because of the stronger onshore winds, and
274 more subdued on the left side due to prevalence of the offshore winds (Simpson &
275 Riehl, 1981). Previous paleohurricane studies have suggested that the proxy record is
276 more sensitive to major hurricanes (category 3 intensity and above) making landfall
277 immediately to the west of the study site (i.e., landfall within 50-km radius) (Liu,
278 2004, 2013; Liu & Fearn, 1993, 2000). Therefore, hurricanes and winter storms that
279 made landfall at the Atlantic Coast or Florida Keys likely will not cause marine
280 incursions detectable in proxy records from the Shark River Estuary. Although 15
281 hurricanes struck the Everglades since the 20th century, only four made landfalls
282 immediately to the north of our study site prior to the coring date (Hurricane Donna,
283 Isbell, Wilma, and the 1948 hurricane) (Figure. 2). Among these four hurricanes,
284 Donna (1960) was a category 3 hurricane at landfall (Houston & Powell, 2003). It
285 travelled parallel to the coastlines of our study area, and struck near Naples and Fort
286 Myers, Florida (Dunn & Miller, 1961). As a result, higher storm surge and damages
287 occurred at the Everglades City (~75 km north of our study site) but not at the Shark
288 River Slough (Craighead & Gilbert, 1962; Smith et al., 2009). Isbell (1964) made
289 landfall as a Category 2 hurricane at ~60 km north of our study site (Dunn, 1965), and
290 no major storm surge was reported (Dunn, 1965). The 1948 hurricane was very
291 similar to hurricane Isbell in its path and intensity (NOAA, 2019). Therefore, it is
292 likely that Hurricane Wilma, being a stronger and more recent storm with a more
293 direct impact at our study site, is the only storm that is individually distinguishable in
294 the sediment profiles from the Shark River Estuary among the 15 major hurricanes
295 recorded in the instrumental record.

296
297 Given the depositional and sea level history of our study area, it is reasonable to
298 believe that the relative site-to-sea distance at site SRM has been sensitive enough to
299 register major hurricane events since ~3500 cal yr BP, when shoreline retreat
300 stabilized at the Shark River Estuary (Yao & Liu, 2017, 2018). Although the sediment
301 profile at the study area recorded over ~5700 years of paleoecological history (Yao et
302 al., 2015), a combination of XRF and isotope analyses is expected to provide a
303 conservative, minimal record of intense hurricanes events over the last 3500 years
304 from core SRM-1. The significance testing of the 45 surface samples from a transect
305 with progressively thinning Hurricane Wilma deposits (Figure. 1) will reveal the
306 sensitivity of various geochemical parameters in relation to marine incursion events.

307

308 **2.3 Methods**

309 **2.31 Core and Surface Sample Extraction**

310 In this study, a 525 cm core (SRM-1) was retrieved using a Russian peat borer along
311 with two 50 cm aluminum push cores at mouth of the Shark River Slough (site SRM)
312 in May 2010 (Figure. 1). In addition, forty-five surface samples were also collected
313 following the channel of the Shark River Slough along a distinct marine-to-terrestrial
314 gradient (Table 1, Figure.1) (Castañeda-Moya et al., 2010; Yao & Liu, 2018). The
315 surface samples were taken from four main study sites (SRM, SRS-6, SRS-5, and
316 SRS-4) ranging from the mouth of the Shark River Slough to ~20 km upstream. At

317 each site, six to sixteen surface samples were taken along a secondary gradient
318 perpendicular to the river as a function of the distance away from the river (Figure. 1),
319 which acts as a conduit of storm surge and storm deposits from the sea (Castañeda-
320 Moya et al., 2010; Chen & Twilley, 1999a, 1999b; Yao & Liu, 2018). A total of 18
321 samples was collected from the four main study sites. Salinity data for site SRS-6 to
322 SRS-4 were retrieved from our collaborators (Castañeda-Moya et al., 2010, 2013,
323 2020). Salinity data for site SRM were measured during our field expedition in May
324 2010. The surface samples were collected by first removing plant litter and debris
325 from the surface ground, and then collecting up to 5 cm of upper soil by using a small
326 hand shovel.

327 328 **2.32 Laboratory analyses**

329 In the laboratory, XRF analysis was performed on all surface samples as well as on
330 core SRM-1 at 2 cm intervals by using an Olympus Innov-X DELTA Premium XRF
331 analyzer, which measures the elemental concentrations of 25+ elements (units are
332 reported in part per million) with an atomic number larger than 15. A total of 15
333 elements was detected in our samples, but 7 of them were in traceable amount with no
334 systematic changes. Therefore, eight common chemical elements (Ca, Sr, S, Fe, Cl,
335 Ti, Zr, and Br) and Cl/Br ratio were reported in this study (Figure. 5).

336
337 In addition, ninety-five samples throughout core SRM-1 at 2 to 5 cm intervals were
338 sent to Stable Isotope Facility at the University of California, Davis for Total Organic
339 Carbon (TOC), $\delta^{13}\text{C}$, and C/N measurements. All the samples consist of bulk
340 sediments. Pretreatment was performed in LSU Global Paleoecology Laboratory,
341 where samples were bathed in 2 ml of 10% HCL, treated in ultrasonic tank for 5
342 minutes, and washed with distilled water and centrifuged for three times for four
343 minutes each. In UC Davis Stable Isotope Facility, samples were analyzed using a
344 PDZ Europa ANCA-GSL elemental analyzer interfaced to a PDZ Europa 20-20
345 isotope ratio mass spectrometer (Sercon Ltd., Cheshire, UK). The isotope data are
346 expressed on a Vienna Pee Dee Belemnite (VPDB) scale.

347
348 Standardization of the selected dataset was used to filtered the “background noises”
349 from sea-level fluctuations and small-scale events and amplify the chemical signals of
350 intense hurricanes. Normalized values of $\delta^{13}\text{C}$, C/N, and selected XRF data were
351 calculated using Z-values (Salkind, 2010). First, we subtracted the mean value of each
352 dataset to each score, and then we divided each result by the standard deviation of the
353 dataset. The standardized dataset was presented to identify periods with higher
354 variability and be comparable with other studies with different proxies. In this paper
355 we focus on the top 445 cm of the core because it contains the depositional history of
356 the peat-forming coastal wetlands that is relevant to the reconstruction of
357 paleohurricane activities.

358 359 **2.33 Statistical analyses**

360 Principal component analysis (PCA) was performed by using the C-2 version 1.8
361 (species transformation: log10, rotate axes, center data by variables, standardize data
362 by variables) on all surface samples to reveal the sensitivity of various geochemical
363 parameters in relation to storm deposits from a modern hurricane event. The PCA
364 results provide a basis to identify the most sensitive geochemical parameter to marine
365 incursion events.

366

367 **2.34 Chronology**

368 Fourteen samples from core SRM-1 were sent to NOSAMS Laboratory at Woods
369 Hole Oceanographic Institution and Beta Analytic Inc., in Miami, Florida for AMS
370 ^{14}C measurements. The chronology of core SRM-1 was developed by using BACON
371 version 2.2 (Blaauw & Christen, 2013) and has been previously established (Yao et
372 al., 2015). The accumulation rate priors are based on default settings (acc.shape=1.5,
373 res=5, mem.strength=4, and mem.mean=0.7), except for prior distributions
374 (acc.mean=10). The ages described in this paper are reported as calibrated years
375 before present (cal yr BP). Because the top 10 cm of the clastic sediments at our study
376 site has been attributed to sediments deposited by Hurricane Wilma in 2005 and
377 published in many studies (Smith et al., 2009; Castañeda-Moya et al., 2010; Smoak et
378 al., 2013; Yao et al., 2015; Yao & Liu, 2017), we used 10-11 cm from the top of core
379 SRM-1 as -55 cal yr BP (1950 AD as 0 cal yr BP) to run the model in BACON
380 version 2.2 (Figure. 4). More information of ^{14}C samples are described in online
381 supplementary content (Table S2).

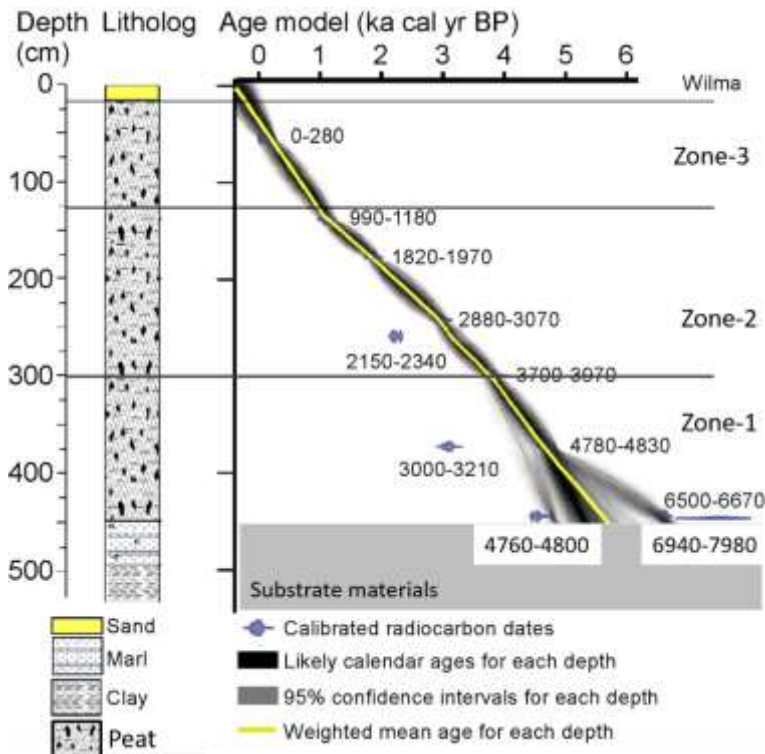
382

383 **3. Results**

384 **3.1 Chronology**

385 Among the 14 AMS ^{14}C dates obtained from NOSAMS and Beta Analytic, three
386 anomalously young dates retrieved at 246 cm and 440 cm are rejected due to extreme
387 stratigraphic reversal (Table S2). The surface (0 cm at -55 cal yr BP) and 11 valid ^{14}C
388 dates were used to construct the age-depth model by BACON v2.2 (Figure. 4). The
389 result shows that the highest probability age-depth model (yellow curve) based on
390 weighted mean age of each depth is very close to a polynomial line intercepting ^{14}C
391 dates at 56 (178 cal yr BP), 139 (1138 cal yr BP), 179 (1872 cal yr BP), 243 (2947 cal
392 yr BP), 300 (3777 cal yr BP), and 374 (4658 cal yr BP) cm. We picked a basal date of
393 5674 cal yr BP at 450 cm based on estimation of the highest probability age-depth
394 model. More detailed description of the chronology of core SRM-1 can be seen in
395 Yao et al. (2015).

396



397

398

399 **Figure 4.** Lithology and the age-depth model for core SRM-1. The age-depth model is developed by
 400 BACON and based on 11 calibrated C^{14} ages (2- σ Calibrated range). The yellow curve shows the
 401 'highest probability' estimated age for each depth based on the weighted mean age.

401

402

3.2 Geochemical Proxy Results

403

404

405

406

407

408

409

410

411

412

3.2.1 Zone-1 (445-300 cm, ~5700-3500 cal yr BP)

413

414

415

416

417

418

419

420

421

422

423

424

425

426

427

Pollen records from previous studies show that the vegetation at our study area was dominated by upland and marsh plants (e.g., *Pinus*, *Quercus*, *Salix*, Poaceae, and Amaranthaceae), suggesting a relatively inland and freshwater environment during this period at our coring site (SRM-1), but the shoreline was closing in due to rapid sea level rise (Yao et al., 2015; Yao & Liu, 2017). The peat sediments in this section display relatively stable geochemical signals throughout Zone-1. The XRF data show that the elemental concentrations of Ca (< 1000 ppm), S (< 5000 ppm), Cl (< 10000 ppm), and Fe (< 2000 ppm) are relatively stable in most intervals throughout Zone-1. Only trace amount of, Ti (< 100 ppm), Sr (< 50 ppm), Zr (< 10 ppm), and Br (< 25 ppm) are detected in some intervals in Zone-1 (Figure. 5). The elemental concentrations of Ca, S, Zr, Cl are in general the lowest throughout the core, and the Cl/Br ratio is relatively higher toward the bottom of Zone-1. In addition, Zone-1 contains the highest TOC% throughout the core. The $\delta^{13}C$ ranges from -28‰ to -25.5‰ and becomes more positive toward the top of the zone. The C/N ranges from 18 to 29.

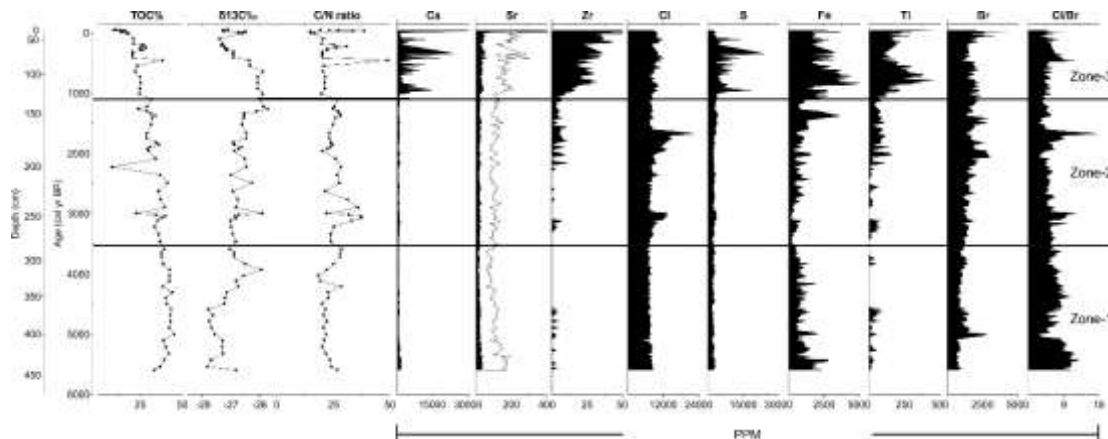


Figure 5. The TOC%, $\delta^{13}\text{C}$, C/N, and XRF diagram of core SRM-1.

429

430

431

432 3.22 Zone-2 (300-125 cm, ~3500-1150 cal yr BP)

433 Although marine transgression has stabilized since ~3500 cal yr BP in South Florida
 434 (Parkinson, 1989; Scholl et al., 1969; Wanless et al., 1994), saltwater intrusion
 435 continued at our study area during the next 2350 years as the freshwater environment
 436 gradually transit to a brackish environment and mangroves started to expand toward
 437 more inland and upstream areas of the Shark River Slough (Yao et al., 2015; Yao &
 438 Liu, 2017). The XRF data show that although still relatively low, the concentration of
 439 most elements has increased in regards to Zone-1, in particular, the concentration of
 440 Zr, Ti, and Br shows substantial increase, and abrupt increases in Cl (>15000 ppm)
 441 and Cl/Br ratio occur at two intervals at approximately 245-260 cm (3000-3400 cal yr
 442 BP) and 160-180 cm (1500-2200 cal yr BP) (Figure. 5). In addition, the TOC%
 443 gradually decreases toward the top of the zone. The $\delta^{13}\text{C}$ ranges from -27‰ to -25‰
 444 and C/N ranges from 20 to 35.

445

446 3.23 Zone-3 (125-0 cm, 1150 cal yr BP to present)

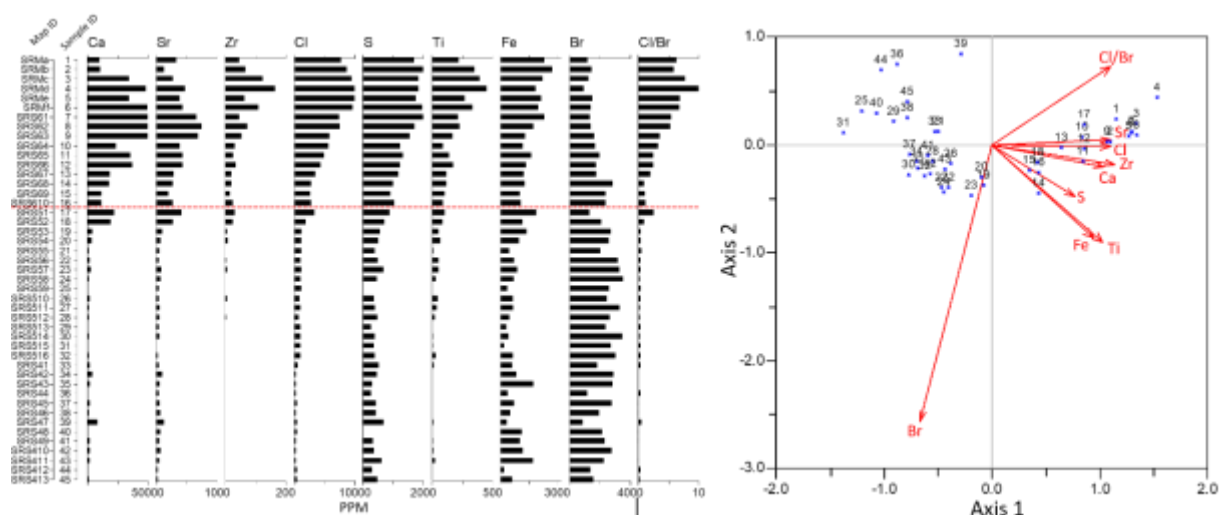
447 The paleoenvironmental history of this period is characterized by the formation of the
 448 modern shoreline, a coastline dominated by *Rhizophora mangle*. XRF analyses show
 449 that the concentrations of all the elements are much higher than those in Zone-1 and
 450 Zone-2. In particular, the top 10 cm of the core contains exponentially higher
 451 concentrations of most elements than in the underlying peat (Figure. 5). The Cl/Br
 452 ratio exhibits some fluctuations throughout Zone-3 (Figure. 5). In addition, the TOC%
 453 further decreases toward the top and reaches the lowest values at the top 10 cm of the
 454 core. The values of $\delta^{13}\text{C}$ and C/N are within the similar range in regard to Zone-2 but
 455 exhibit more variations.

456

457 3.3 Numerical Analysis of Surface Samples

458 XRF analysis of the 45 surface samples show that samples taken from site SRM-1 and
 459 SRS-5 have higher concentration of all measured elements in regard to samples from
 460 site SRS-5 and SRS-4. In particular, samples from site SRM-1 have significantly
 461 higher Cl, S, Ti, Fe, Br, and Cl/Br ratio than all the other surface samples. Overall, the
 462 chemical richness decreases progressively from site SRM-1 to SRS-4 (Figure. 6).
 463 The XRF data of all 45 surface samples were used in PCA analysis. On the PCA
 464 biplot of the 9 chemical parameters (Fig. 4), the first two principal components (PC)
 465 account for 71.3% and 9.7% of the variance (Table S3). All samples from Site SRM-1
 466 and most samples from site SRS-6 have positive scores on both PC1 and PC2 axes

467 and are located in the upper-right quadrant of the biplot (Figure. 6). Among all the
 468 variables, Cl/Br, Sr, and Cl have positive scores on both PC1 and PC2 axes and Br
 469 has negative scores on both PC1 and PC2 axes.
 470



471
 472 **Figure 6.** Left: XRF results of 8 chemical elements and Cl/Br ratio for 45 surface samples. Samples
 473 coded to aid the identification. Same coding applies to the map and all the other figures. The red line
 474 separates samples from coastal (SRM, SRS-6) and terrestrial (SRS-5, SRS-4) sites. Right: PCA biplot
 475 showing coordinates of 8 chemical elements and Cl/Br ratio from the XRF diagram of surface samples
 476 plotted along component 1 and component 2.
 477

478 4. Discussion

479 4.1 Significance testing of the marine indicators in relation to Hurricane Wilma

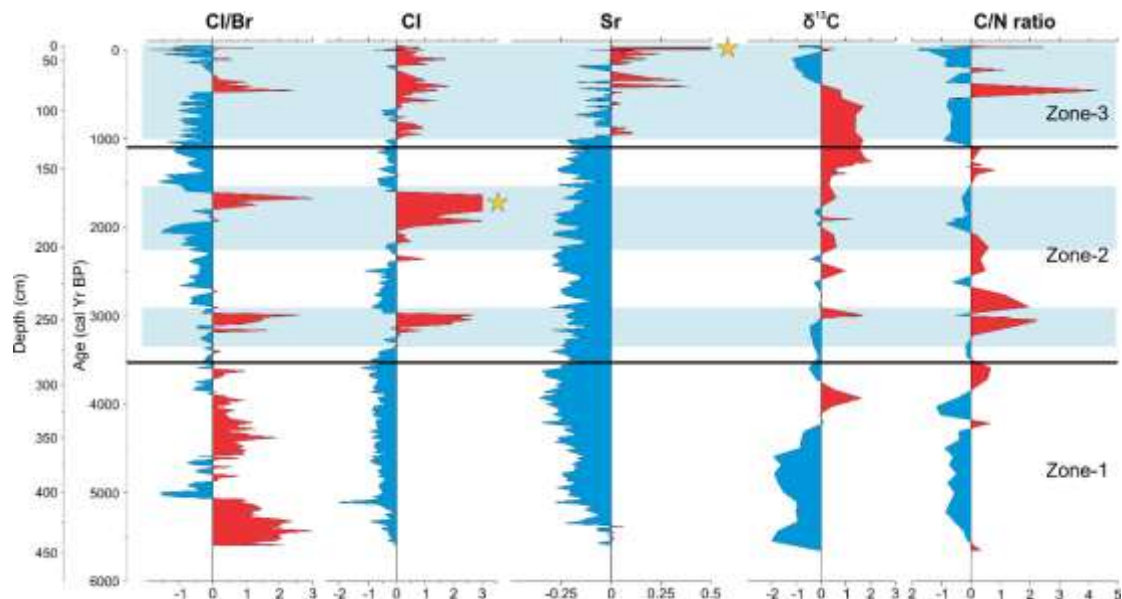
480 Previous studies have thoroughly described that storm surge and associated deposition
 481 from Hurricane Wilma caused significant impacts to coastal areas along the Shark
 482 River Slough (site SRM and SRS-5) (Castañeda-Moya et al., 2010, 2020; Smith et al.,
 483 2009; Smoak et al., 2013; Yao et al., 2015; Yao & Liu, 2017, 2018). More
 484 importantly, Hurricane Wilma was the only major hurricane that landed directly
 485 across our study area prior to the coring date. Thus, it can be inferred that the top 10
 486 cm of calcareous clastic sediments in core SRM-1 and surface samples from site SRM
 487 and SRS-6 are the storm deposits from Hurricane Wilma (Figures 5 & 6).
 488

489 Figure 6 summarizes the geochemical characteristics of the storm deposits. Overall,
 490 the Wilma deposits have significantly higher contents of Zr, Ca, Sr, Ti, Cl, S, and
 491 Cl/Br ratio and slightly higher concentration of Fe than the underlying peat (Figures 5
 492 & 6). In particular, significance testing of the surface samples taken along a marine-
 493 to-terrestrial gradient with gradually thinning storm signals shows that the elemental
 494 concentration of Cl and Sr and Cl/Br ratio have the closest association with storm
 495 deposits from Hurricane Wilma among the 9 XRF parameters. High content of Sr has
 496 been described as an indicator of marine incursions in previous studies from
 497 southwestern Florida (Van Soelen et al., 2012; Yao & Liu, 2018) and elsewhere
 498 (Bianchette et al., 2016; Liu et al., 2015; McCloskey et al., 2015; McCloskey et al.,
 499 2018; McCloskey & Liu, 2013; Ramírez-Herrera et al., 2012; Woodruff et al., 2009).
 500 This element is likely associated with marine gastropods in offshore environment and
 501 introduced to coastal area by storm surges (Yao et al., 2015, 2019; Yao & Liu, 2017).
 502 The ratio of Cl/Br has the highest score on both PC1 and PC2 axes, hence it has the
 503 closest association with Wilma deposits. Many studies have revealed that although
 504 aqueous bromine (HOBr/OBr-) is one of the most abundant element in seawater, it

505 tends to react with organic matters in terrestrial environments, due to its higher
506 electron density and smaller bond strength (Westerhoff et al., 2004; Ryu et al., 2018).
507 On the contrary, chlorine (HOCl/OCl⁻) is more abundant in inorganic environments
508 (Donahoe et al., 1994; Thuthill et al., 1998). Hence, an increase in Cl and decrease in
509 Br concentration has been used as evidence for marine incursion event (e.g., storm
510 surge) in highly organic environment (e.g., coastal wetland). Furthermore, The Cl/Br
511 ratio in seawater (655:1) (Alcalá & Custodio, 2004) is much higher than that in
512 precipitation (100:1 to 300:1) (Davis et al., 1998). Therefore, the Cl/Br ratio is a
513 sensitive indicator to detect evidence of storm surge in sediment profile (Liu et al.,
514 2015; Yao et al., 2015). In this case, unlike other common marine indicators (e.g., Zr,
515 Ca, Sr, and S) described in previous studies (Bianchette et al., 2016; McCloskey et al.,
516 2015; McCloskey & Liu, 2013; Ramírez-Herrera et al., 2012), the ratio of Cl/Br and
517 the concentration of Cl is associated with saltwater intrusion caused by storm surges
518 (Liu et al., 2015; McCloskey et al., 2018; Yao et al., 2019). More importantly, a study
519 of Hurricane Harvey deposits from the Texas coast has demonstrated that the ratio of
520 Cl/Br can be used to identify storm surge events in the sedimentary record in the
521 absence of overwash processes (Yao et al., 2019). Hence, this parameter is a
522 particularly sensitive storm indicator in sand-limited coastal systems where traditional
523 sedimentological proxies (i.e., overwash sand layers) are absent or ineffective.
524 Therefore, based on the significance testing of surface samples and information from
525 previous studies, we believe that the elemental concentration of Sr and Cl and the
526 ratio of Cl/Br are the most sensitive indicators for major hurricane events at our study
527 area among all nine XRF parameters.
528

529 **4.2 Geochemical Record of Late-Holocene Hurricane Events**

530 Figure 7 summarizes the standardized Cl/Br, Cl, Sr, $\delta^{13}\text{C}$, and C/N data from core
531 SRM-1. Positive excursions in Cl/Br, Sr, and Cl record are marked in red color and
532 interpreted as potential evidence for paleohurricane activities. From ~5700 to 3500 cal
533 yr BP (Zone-1), although Cl/Br record shows many intervals with positive excursions,
534 Cl and Sr record exhibit opposite results. This inconsistency among storm indicators
535 in the dataset is likely caused by sediment compaction and different
536 geomorphological condition during the time period (Yao et al., 2015; Yao & Liu,
537 2017). As discussed in previous sections, site SRM was situated in a relatively inland
538 and freshwater environment prior to 3500 cal yr BP. Although marine transgression
539 was rapidly approaching in, the relative sea level in southwestern Florida was still
540 much lower than the present level and the shoreline was ~30 km seaward relative to
541 that of today (Parkinson, 1989; Wanless et al., 1994; Yao et al., 2015). With such site-
542 to-sea distance, sediment profiles in Zone-1 was not sensitive enough to register any
543 evidence of paleohurricane activities between ~5700 to 3500 cal yr BP. More
544 importantly, because bromine originates almost exclusively from seawater
545 (Westerhoff *et al.*, 2004; McCloskey et al., 2018), it is reasonable to believe that the
546 concentration of this element is remarkably lower in the sediment profile prior to
547 3500 cal yr BP when the sea level was lower than today. Hence, the high Cl/Br ratio,
548 which pervades virtually throughout the entire Zone-1, rather than episodically as in
549 the two zones above it, is caused by the lowered Br concentrations here relative to the
550 consistent Cl values (Figure 5). This suggests that the high Cl/Br ratio reflects the
551 geochemical and environmental background at the site and cannot be taken as a
552 paleohurricane proxy during these two millennia.
553



554 **Figure 7.** Cl/Br, Cl, Sr, $\delta^{13}\text{C}$, and C/N records for core SRM-1. The data have been standardized and
 555 plotted by positive (red) and negative (blue) excursions from the mean concentrations of each variable.
 556 Intervals marked by blue shades represent periods of elevated major hurricane activities (category 3-5).
 557 The star points to intervals with exponentially high values where the curve was cut off to save space.
 558 Sediments deposited by Hurricane Wilma is represented by a thin peak of high values of Cl/Br, Sr, and
 559 C/N at the top of the core.
 560

561

562 From 3500 to 1150 cal yr BP (Zone-2), although the Sr record still shows negative
 563 excursions, many intervals in the Cl/Br and Cl records show signs of marine
 564 incursions. In particular, two prominent peaks occur between 245-260 cm (~3000-
 565 3400 cal yr BP) and 160-180 cm (~1500-2200 cal yr BP) (Figure. 7). We interpret
 566 that these two intervals represent two periods of elevated major hurricane activities
 567 (category 3-5). Previous observational and modeling studies suggest that major
 568 hurricanes can introduce marine water and sediments up to 10 km inland in the coastal
 569 Everglades (Castañeda-Moya et al., 2010, 2013; Chen & Twilley, 1999b; Smith et al.,
 570 2009; Smoak et al., 2013). During Zone-2, although much closer to the sea in
 571 comparison to Zone-1, our study site, which is currently at the mouth of the Shark
 572 River Slough, would still have been at some distance inland from the former shoreline
 573 and beyond the distance reachable by marine sediments carried by storm surge waters
 574 during the period from ~3500 to 1150 cal yr BP. This explains the negative
 575 background values of Sr, a common indicator of marine sediments (Bianchette et al.,
 576 2016; McCloskey et al., 2015; McCloskey & Liu, 2013; Ramírez-Herrera et al., 2012;
 577 Yao & Liu, 2018), throughout Zone-2. However, Cl and Cl/Br are associated more
 578 with saltwater intrusion than the delivery of marine sediments (Liu et al., 2015;
 579 McCloskey et al., 2018; Yao et al., 2019). Hence, extremely high-energy events, such
 580 as strong storm surges caused by catastrophic hurricanes (category 4 or 5) could have
 581 introduced large quantities of seawater to the coring site, and the impoundment of the
 582 storm surge water inland by natural topographic barriers is reflected by positive
 583 excursions of Cl and Cl/Br in Zone-2.
 584

585

586 From 1150 cal yr BP to present (Zone-3), as sea level rise has rendered the study site
 587 a truly coastal location subjected to storm surge deposition (Yao et al., 2015),
 588 intervals with positive excursion of Cl/Br, Cl, and Sr increase exponentially in Zone-3
 589 (Figure. 7). In particular, three intervals from ~1000 to 800 cal yr BP, ~600 to 300 cal
 yr BP, and ~150 cal yr BP to present exhibit very high hurricane activities.

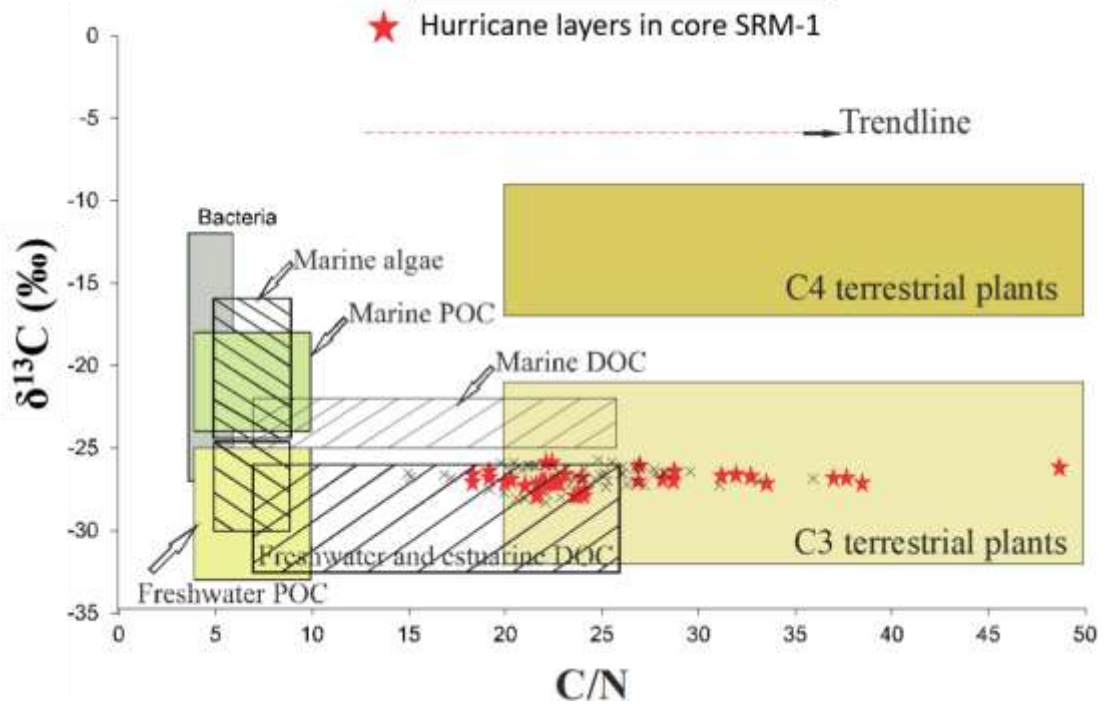
590 Coincidentally, the modern dense mangrove forest in southwestern Florida was
591 established during the last millennia (Yao et al., 2015; Yao & Liu, 2017). Therefore, it
592 is reasonable to believe that the increased mineral and sediment inputs due to elevated
593 hurricane activities after 1150 cal yr BP likely enhanced nutrient availabilities in the
594 Shark River Estuary and played an important role in the development of the mangrove
595 forests at our study area (Castañeda et al., 2020).

596

597 Overall, the geochemical datasets of core SRM identified 5 active periods of intense
598 hurricane activities during the last 3500 years at ~3400-3000, ~2200-1500, ~1000-
599 800, ~600-300, and ~150 cal yr BP to present (Figure. 7). This is the longest
600 paleohurricane record to date from South Florida. This study also demonstrates that
601 geochemical signals, in particular, signals of saltwater intrusion can be preserved in
602 the sediment profiles on millennial time-scale and measured by selected XRF
603 variables, thereby enabling more storm records to be produced from otherwise
604 suboptimal sand-limited coastal systems such as the Florida Everglades. This
605 methodological advancement has the potential to connect the existing hurricane
606 records in the regional context to examine the long-term hurricane dynamics at a
607 regional scale.

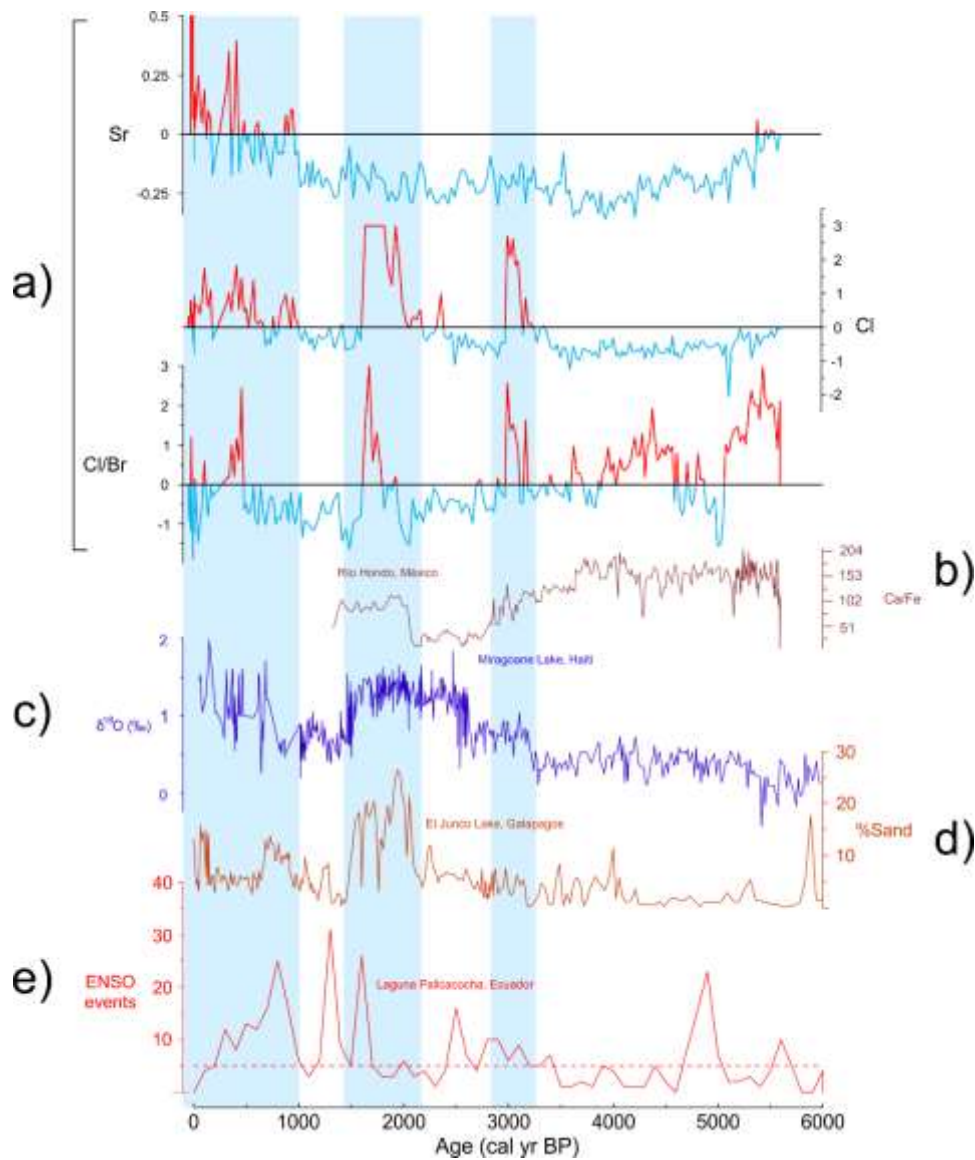
608

609 For the isotopic results, previous studies have indicated that marine-originated organic
610 materials, hence storm deposits, contain more positive $\delta^{13}\text{C}$ and lower C/N values
611 (Figure. 8) (Chmura & Aharon, 1995; Das et al., 2013; Lamb et al., 2006; Lambert et
612 al., 2008). However, the inferred storm intervals show very inconsistent $\delta^{13}\text{C}$ and C/N
613 values throughout Zone-2 and Zone-3 (Figure. 7), and most intervals in core SRM-1
614 fall within the range of C3 terrestrial plants instead of marine originated sources
615 (Figure. 8). We think this discrepancy is caused by high contents of mangrove peat in
616 the core. In our study area, the scarcity of clastic material (especially sand) and peat-
617 dominated sediment profiles contributed to high content of TOC throughout core
618 SRM-1 (Figure. 5). More importantly, the peat deposition at the mouth of the Shark
619 River Slough was mainly contributed by autochthonous accumulation from the
620 mangrove forests since ~3500 cal yr BP (Lodge, 2016; Parkinson, 1989; Yao et al.,
621 2015; Yao & Liu, 2017). In the Everglades, all three mangroves species include
622 *Laguncularia racemosa*, *Rhizophora mangle*, and *Avicennia germinans* are C3 plants.
623 It is likely that strong $\delta^{13}\text{C}$ and C/N signals contributed by organic materials from
624 mangrove peat overwhelm the occasional hurricane signals in the sediment profile.



625
 626 **Figure 8.** Typical $\delta^{13}\text{C}$ and C/N ranges for organic materials from various sources in coastal
 627 environments (Lamb et al., 2006). Red stars mark the isotope datasets of inferred storm intervals in
 628 core SRM-1. The rest of the sediment intervals in core SRM-1 are marked by "X".

629
 630 **4.3 Climatic Forcing and Late-Holocene Hurricane Activities in the Florida**
 631 **Everglades**
 632



633
 634 **Figure 9.** Paleohurricane record from a) core SRM-1 comparing with other paleoenvironmental
 635 reconstructions from across the Caribbean and Eastern Pacific. b) Precipitation record during the mid-
 636 to Late-Holocene from southeastern Yucatan Peninsula (Aragón-Moreno et al., 2018); c) Holocene
 637 climate reconstructions of Lake Miragoane, Haiti based on $\delta^{18}\text{O}$ record (Hodell et al., 1991); d) ENSO
 638 intensifications during the Holocene interpreted by sand record from El Junco Lake, Galapagos
 639 (Conroy et al., 2008); e) Total ENSO events modelled by 100 years overlapping window from Laguna
 640 Pallacocha, southern Ecuador (Moy et al., 2002). Intervals shaded in blue represent periods of
 641 elevated intense hurricane activities, ENSO intensifications, and increased precipitation in the
 642 Caribbean and Florida.

643
 644 Our paleohurricane record from the Everglades documented five active periods of
 645 intense hurricane activities at ~3400-3000, ~2200-1500, ~1000-800, ~600-300, and
 646 ~150 cal yr BP to present. Many studies from across the GOM and Caribbean Basin
 647 have attributed the periodic changes in the regional climatic patterns (e.g.,
 648 precipitation and hurricanes) during the Late-Holocene to variations of the
 649 Intertropical Convergence Zone (ITCZ) position, the position and strength of the
 650 Bermuda High or NAO, and/or intensification of the El Niño/Southern Oscillation
 651 (ENSO) (e.g., Aragón-Moreno et al., 2018; Baldini et al., 2016; Donnelly &
 652 Woodruff, 2007; Hodell et al., 1991; Elsner et al., 2000; Liu and Fearn, 2000;
 653 McCloskey & Liu, 2012 a & b). In addition to these large-scale climatic controls, it is

654 important to point out that our study site, situated on the Gulf Coast of the Everglades,
655 is affected by intense hurricanes coming from both the Atlantic Ocean to the east (i.e.,
656 the Cape Verde hurricanes) and the Gulf of Mexico to the west (i.e., the
657 baroclinically-enhanced hurricanes, such as Hurricane Wilma) (Elsner et al., 1996)
658 (Figure 2). Therefore, the paleohurricane history of our study site may reflect the
659 complex interactions among the different climatic mechanisms affecting the activity
660 of the Cape Verde hurricanes versus the baroclinically-enhanced hurricanes either
661 concurrently or asynchronously. Figure 9 shows our proxy-indicated activity periods
662 plotted alongside some key paleoclimatic proxy records from the Caribbean and
663 broader neotropical regions.

664
665 The first active period, ~3400-3000 cal yr BP, coincides with a distinct rise in $\delta^{18}\text{O}$
666 values at Lake Miragoane, Haiti (Figure 9c), interpreted to signal an abrupt shift
667 towards a drier climate in the Caribbean (Hodell et al., 1991). This climatic change
668 has been attributed to a southwestward shift of the Bermuda High, the subtropical
669 anticyclone that steers many Cape Verde hurricanes from the tropical Atlantic Ocean
670 towards North America (Liu and Fearn, 2000). Consequently, more hurricanes were
671 steered towards the Gulf of Mexico and the Caribbean region after 3800 cal yr BP,
672 marking the onset of a hyperactive period in intense hurricane landfall detected in the
673 paleotempestology records across the northern Gulf of Mexico coast (Liu, 2004). It is
674 remarkable that the onset of heightened hurricane activity seemed to occur
675 synchronously across the Gulf Coast, even down to the Everglades. It also coincided
676 with a southward shift of the ITCZ around 3500 cal yr BP (Haug et al., 2001). Thus,
677 the paleoclimatic records seem to support that the 3400-3000 cal yr BP active period
678 in the Everglades was part of a large-scale atmospheric circulation changes that
679 involved a southward shift of the ITCZ and the Bermuda High around 3500 years ago.

680
681 The second active period, ~2200-1500 cal yr BP, coincided with an abrupt increase in
682 the Ca/Fe elemental ratio in the Rio Hondo record from the southeastern Yucatan
683 Peninsula (Figure 9b), interpreted to reflect increased precipitation in the western
684 Caribbean (Aragón-Moreno et al., 2018). Hurricane landfall along the northern Gulf
685 of Mexico coast continued to be high (Liu, 2004; Bregy et al., 2018). At the same
686 time, ENSO activity increased to the highest level during the late Holocene (Conroy
687 et al., 2008), while the climate in Haiti remained dry (Hodell et al., 1991) (Figure 9c-
688 9d). One possible scenario is that the elevated activity recorded in the southwestern
689 Everglades during this period was due to an increase in baroclinically-enhanced
690 hurricanes spawned from the Gulf of Mexico and the western Caribbean. The coupled
691 effects of ITCZ movements and ENSO intensification on precipitation and hurricane
692 activity in the Gulf of Mexico region are complex and not well known (Aragón-
693 Moreno et al., 2018). More work is needed to evaluate this hypothesis.

694
695 All three of the youngest active periods occurred within the last millennium. Thus the
696 period 1000-0 cal yr BP can be broadly regarded as a relatively active period. The
697 interval of ~900-600 was also identified as a time of high hurricane activity in a proxy
698 record near Naples, southwestern Florida, only 80 km north of our study site (Ercolani
699 et al., 2015). By contrast, the last millennium was shown to be an inactive period
700 marked by few intense hurricane landfalls on the northern Gulf Coast (Liu, 2004). A
701 southward retreat of the ITCZ, as documented from the Cariaco Basin (Haug et al.,
702 2001), would have caused a shift of the predominant storm tracks to the south,
703 bringing fewer hurricanes to the northern Gulf Coast but more to the Everglades and

704 to as far south as Nicaragua (McCloskey and Liu, 2012). On the other hand, the past
705 millennium seemed to be marked by moderately high ENSO activity in general, albeit
706 with great variability (Conroy et al., 2008; Moy et al., 2002) (Figure 9d-9e). On the
707 sub-millennial level, the three active hurricane periods identified in our study site
708 (~1000-800, 600-300, 150-0 cal yr BP) seem to correspond with intervals of relatively
709 low ENSO activity (Figure 9d-9e). Today, hurricane risks in South Florida are highest
710 during years of positive Southern Oscillation Index (SOI) (or La Nina) and negative
711 NAO (Elsner and Bossak, 2004). The apparent negative relationship between
712 hurricane activity levels at our study site and the frequency of ENSO events suggests
713 that hurricane activity regimes in South Florida have been modulated by the interplay
714 among the ITCZ, ENSO, and NAO for at least the past millennium. It is likely that
715 other regional climatic and oceanographic variables, such as the Loop Current and the
716 Atlantic Multi-decadal Oscillation (AMO, which is largely a function of sea surface
717 temperature in the tropical and subtropical Atlantic Ocean), may have played a
718 significant role too (Goldenberg et al., 2001; Bregy et al., 2018).

719
720 In addition, the overall values of the marine indicators (Ca, Sr, Zr) all increased after
721 ~1000 cal yr BP in core SRM-1 (Figure 5), approximately when the shoreline reached
722 its modern position at the Shark River Estuary (Yao et al., 2015). We believe these
723 marine sediments are likely carbonate materials contributed by small-scale events
724 (e.g., winter storms and minor tropical cyclones) that produced an amalgamated
725 deposit of material over time with the same chemical signals as deposits from intense
726 hurricanes. As the approximate distance of site SRM-1 to the Gulf was relatively
727 closer in the last millennia, our study area became more sensitive to receive and
728 preserve deposits from these small-scale events in the sedimentary profile. However,
729 the remarkable chemical imprints from the intense hurricanes such as Wilma is still
730 clearly distinguishable as shown in the standardized datasets in Figure 7.

731
732 Many proxy-based paleohurricane records have been published from study sites along
733 the Gulf Coast and the Caribbean in recent years (Baldini et al., 2016; Brandon et al.,
734 2013; Bregy et al., 2018; Burn & Palmer, 2015; Das et al., 2013; Denommee et al.,
735 2014; Donnelly & Woodruff, 2007; Ercolani et al., 2015; Frappier et al., 2007, 2014;
736 van Hengstum et al., 2014; Lane et al., 2017; Lane et al., 2011; LeBlanc et al., 2017;
737 Liu et al., 2008; McCloskey & Liu, 2012 a&b, 2013; Park, 2012; Wallace et al., 2014;
738 Wallace & Anderson, 2010). These studies generally show multi-centennial periods of
739 significantly increased hurricane activity separated by quieter inactive periods during
740 the Late-Holocene. Two hypotheses exist regarding the temporal correlations between
741 the Late-Holocene active/inactive hurricane periods and the climatic forcing
742 mechanisms. One group of views is that hurricane regimes are synchronous across the
743 entire North Atlantic basin because hurricane activity levels are controlled by large-
744 scale forcing mechanism such as ENSO, which affects the entire basin (Donnelly &
745 Woodruff, 2007; Mann et al., 2009). Another group of views is that hurricane
746 regimes are not synchronous across the North Atlantic; but instead, they show anti-
747 phase or time-transgressive patterns across geographical regions as a result of
748 latitudinal shifts in predominant storm tracks driven by changing positions or
749 strengths of the ITCZ, Bermuda High, or NAO (Baldini et al., 2016; Elsner et al.,
750 2000; Liu, 2004; Liu and Fearn, 2000; McCloskey and Liu, 2012; McCloskey et al.,
751 2013). Our paleohurricane record is broadly in line with hurricane regimes inferred
752 from records from Hancock County, Mississippi (Bregy et al., 2018), Apalachee Bay,
753 North Florida (Lane et al., 2011), Southwest Florida (Ercolani et al., 2015), Belize

754 (Denommee et al., 2014; McCloskey & Liu, 2012a), and Nicaragua (McCloskey &
755 Liu, 2012b). Although the timing and length of the various active hurricane periods
756 among the above records vary, the age gaps may be caused by various
757 geomorphological and meteorological factors, dating control, and sensitivity of
758 different study sites, rather than variations of the climatic forcing.

759

760 **5. Conclusion**

761 In this study, geochemical datasets from core SRM-1 and significance testing of 45
762 surface samples from the Shark River Estuary identified 5 active periods of intense
763 hurricane activities during the last 3500 years at ~3400-3000, ~2200-1500, ~1000-
764 800, ~600-300, and ~150-0 cal yr BP. Our results support the notion that intense
765 hurricane activities in South Florida and the Gulf of Mexico/western Caribbean region
766 was modulated by ITCZ movements, ENSO activities, and the NAO during the Late-
767 Holocene. This study presents the longest hurricane record to date from South Florida.
768 Hence, it fills an important data gap in the paleotempestology data network between
769 the GOM and Atlantic Coasts of the U.S and the Caribbean region. This study also
770 contributes to the methodological advancement of paleotempestology by exploring
771 the application of geochemical proxies in non-limnic, sand-limited, mangrove-
772 dominated tropical coastal wetlands. Further paleoecological studies are needed to
773 produce a high-resolution multi-proxy record that integrates geochemical,
774 sedimentological, and palynological data for a better understanding of the post-storm
775 process of forest succession and ecosystem recovery in the Everglades during the
776 Late-Holocene. More work also needs to be done to explore the use of geochemical
777 and isotopic analyses in detecting storm signals from sand-limited coastal
778 environments.

779

780 **Acknowledgements**

781 This research was supported by grants from the U.S National Science Foundation
782 (Grants #1759715, 1212112, and NSF DDRI Grant # BCS-1303114) and the Inter-
783 American Institute for Global Change Research (IAI #SGP-CRA-2050). We thank
784 T.A. McCloskey for his assistance in fieldwork. Special thanks go to the Florida
785 Coastal Everglades LTER program, the Florida Bay Interagency Science Center-
786 Everglades National Park (FBISC-ENP), and Florida International University for field
787 and logistical support during this study. We also thank four anonymous reviewers
788 who provided valuable comments to improve the manuscript. Data related to this
789 article are open to the public and can be found at the Neotoma Paleocology Database
790 for free (<https://www.neotomadb.org>, Site ID: 10436).

791

792 **References**

- 793 Alcalá, F. J. & Custodio, E. (2004). Use of the Cl/Br ratio as a tracer to identify the
794 origin of salinity in some coastal aquifers of Spain. In: *Groundwater and*
795 *Saltwater Intrusion: Selected Papers from the 18th saltwater intrusion meeting*
796 (ed. by Araguás, L., Custodio, E. & Manzano, M), 481–498. Publicaciones del
797 Instituto Geológico y Minero de España.
- 798 Aragón-Moreno, A. A., Islebe, G. A., Roy, P. D., Torrescano-Valle, N., & Mueller, A.
799 D. (2018). Climate forcings on vegetation of the southeastern Yucatán Peninsula
800 (Mexico) during the middle to late Holocene. *Palaeogeogr. Palaeoclimatol.*
801 *Palaeoecol.*, 495, 214–226.
- 802 Baldini, L. M., Baldini, J. U. L., McElwaine, J. N.,
803 Frappier, A. B., Asmerom, Y., Liu, K.-B., et al. (2016). Persistent northward
North Atlantic tropical cyclone track migration over the past five centuries.

- 804 *Scientific Reports*, 6, 37522.
- 805 Bianchette, T. A., McCloskey, T. A., & Liu, K.-B. (2016). Re-Evaluating the
806 Geological Evidence for Late Holocene Marine Incursion Events along the
807 Guerrero Seismic Gap on the Pacific Coast of Mexico. *PloS One*, 11(8),
808 e0161568.
- 809 Blaauw, M., & Christen, J. A. (2013). Bacon Manual v2. 2. *Blaauw, M., Wohlfarth,*
810 *B., Christen, JA, Ampel, L., Veres, D., Hughen, KA, Preusser, F., et Al.*
811 *(2010),—Were Last Glacial Climate Events Simultaneous between Greenland*
812 *and France*, 387–394.
- 813 Brandon, C. M., Woodruff, J. D., Lane, D. P., & Donnelly, J. P. (2013). Tropical
814 cyclone wind speed constraints from resultant storm surge deposition: A 2500
815 year reconstruction of hurricane activity from St. Marks, FL. *Geochemistry,*
816 *Geophysics, Geosystems*, 14(8), 2993–3008.
- 817 Bregy, J. C., Wallace, D. J., Minzoni, R. T., & Cruz, V. J. (2018). 2500-year
818 paleotempestological record of intense storms for the northern Gulf of Mexico,
819 United States. *Marine Geology*, 396, 26–42.
- 820 Burn, M. J., & Palmer, S. E. (2015). Atlantic hurricane activity during the last
821 millennium. *Scientific Reports*, 5, 12838.
- 822 Cai, W., Santoso, A., Wang, G., Yeh, S.-W., An, S.-I., Cobb, K. M., et al. (2015).
823 ENSO and greenhouse warming. *Nature Climate Change*, 5(9), 849–859.
- 824 Castañeda-Moya, E., Twilley, R. R., Rivera-Monroy, V. H., Zhang, K., Davis, S. E.,
825 & Ross, M. (2010). Sediment and Nutrient Deposition Associated with
826 Hurricane Wilma in Mangroves of the Florida Coastal Everglades. *Estuaries and*
827 *Coasts*, 33(1), 45–58.
- 828 Castañeda-Moya, E., Twilley, R. R., & Rivera-Monroy, V. H. (2013). Allocation of
829 biomass and net primary productivity of mangrove forests along environmental
830 gradients in the Florida Coastal Everglades, USA. *Forest Ecology and*
831 *Management*, 307, 226–241.
- 832 Castañeda-Moya, E., Rivera-Monroy, V.H., Chambers, R.M., Zhao, X., Lamb-
833 Wotton, L., Gorsky, A., Gaiser, E.E., Troxler, T.G., Kominoski, J.S. and Hiatt,
834 M., 2020. Hurricanes fertilize mangrove forests in the Gulf of Mexico (Florida
835 Everglades, USA). *Proceedings of the National Academy of Sciences*, 117(9),
836 pp.4831-4841.
- 837 Chen, R., & Twilley, R. R. (1999a). A simulation model of organic matter and
838 nutrient accumulation in mangrove wetland soils. *Biogeochemistry*, 44(1), 93–
839 118.
- 840 Chen, R., & Twilley, R. R. (1999b). Patterns of mangrove forest structure and soil
841 nutrient dynamics along the Shark River estuary, Florida. *Estuaries*, 22(4), 955–
842 970.
- 843 Chmura, G. L., & Aharon, P. (1995). Stable Carbon Isotope Signatures of
844 Sedimentary Carbon in Coastal Wetlands as Indicators of Salinity Regime.
845 *Journal of Coastal Research*, 11(1), 124–135.
- 846 Conroy, J. L., Overpeck, J. T., Cole, J. E., Shanahan, T. M., & Steinitz-Kannan, M.
847 (2008). Holocene changes in eastern tropical Pacific climate inferred from a
848 Galápagos lake sediment record. *Quaternary Science Reviews*, 27(11–12), 1166–
849 1180.
- 850 Craighead, F. C., & Gilbert, V. C. (1962). The effects of Hurricane Donna on the
851 vegetation of southern Florida. *Quarterly Journal of the Florida Academy of*
852 *Sciences*, 25(1), 1–28.
- 853 Das, O., Wang, Y., Donoghue, J., Xu, X., Coor, J., Elsner, J., & Xu, Y. (2013).

- 854 Reconstruction of paleostorms and paleoenvironment using geochemical proxies
855 archived in the sediments of two coastal lakes in northwest Florida. *Quaternary*
856 *Science Reviews*, 68, 142–153.
- 857 Davis, S. N., Whittemore, D. O. & Fabryka-Martin, J. (1998) Uses of
858 Chloride/Bromide ratios in studies of potable water. *Ground Water* 36, 338–350.
- 859 Denomme, K. C., Bentley, S. J., & Droxler, A. W. (2014). Climatic controls on
860 hurricane patterns: a 1200-y near-annual record from Lighthouse Reef, Belize.
861 *Scientific Reports*, 4, 3876.
- 862 Donnelly, J. P., & Woodruff, J. D. (2007). Intense hurricane activity over the past
863 5,000 years controlled by El Niño and the West African monsoon. *Nature*,
864 447(7143), 465–468.
- 865 Donnelly, J. P., Bryant, S. S., Butler, J., Dowling, J., Fan, L., Hausmann, N., et al.
866 (2001). 700 yr sedimentary record of intense hurricane landfalls in southern New
867 England. *GSA Bulletin*, 113(6), 714–727.
- 868 Donnelly, J. P., Roll, S., Wengren, M., Butler, J., Lederer, R., & Webb, T. (2001).
869 Sedimentary evidence of intense hurricane strikes from New Jersey. *Geology*,
870 29(7), 615–618.
- 871 Dunn, G. E. (1965). The hurricane season of 1964. *Monthly Weather Review*, 93,
872 175–187.
- 873 Dunn, G. E., & Miller, B. I. (1961). The hurricane season of 1960. *Monthly Weather*
874 *Review*, 89(3), 99–108.
- 875 Elsner, J. B., & Bossak, B. H. (2004). Hurricane landfall probability and climate. In
876 R. J. Murnane & K.B. Liu (Eds.), *Hurricanes and Typhoons: Past, Present and*
877 *Future*. New York: Columbia University Press.
- 878 Elsner, J. B., & Kara, A. B. (1999). *Hurricanes of the North Atlantic: Climate and*
879 *Society*. Oxford University Press.
- 880 Elsner, J. B., Lehmiller, G. S., & Kimberlain, T. B. (1996). Objective classification of
881 Atlantic hurricanes. *Journal of Climate*, 9(11), 2880–2889.
- 882 Elsner, J. B., Liu, K. B., & Kocher, B. (2000). Spatial variations in major US
883 hurricane activity: Statistics and a physical mechanism. *Journal of*
884 *Climate*, 13(13), 2293–2305.
- 885 Ercolani, C., Muller, J., Collins, J., Savarese, M., & Squicimara, L. (2015). Intense
886 Southwest Florida hurricane landfalls over the past 1000 years. *Quaternary*
887 *Science Reviews*, 126, 17–25.
- 888 Frappier, A. B., Sahagian, D., Carpenter, S. J., González, L. A., & Frappier, B. R.
889 (2007). Stalagmite stable isotope record of recent tropical cyclone events.
890 *Geology*, 35(2), 111–114.
- 891 Frappier, A. B., Pyburn, J., Pinkey-Drobnis, A. D., Wang, X., Corbett, D. R., &
892 Dahlin, B. H. (2014). Two millennia of tropical cyclone-induced mud layers in a
893 northern Yucatán stalagmite: Multiple overlapping climatic hazards during the
894 Maya Terminal Classic “megadroughts.” *Geophysical Research Letters*, 41(14),
895 5148–5157.
- 896 Gao, S., Jia, J., Yang, Y., Zhou, L., Wei, W., Mei, Y., et al. (2019). Obtaining
897 typhoon information from sedimentary records in coastal-shelf waters. *Haiyang*
898 *Xuebao*, 41(10), 141–160.
- 899 Glaser, P. H., Hansen, B. C. S., Donovan, J. J., Givnish, T. J., Stricker, C. A., &
900 Volin, J. C. (2013). Holocene dynamics of the Florida Everglades with respect to
901 climate, dustfall, and tropical storms. *Proceedings of the National Academy of*
902 *Sciences of the United States of America*, 110(43), 17211–17216.
- 903 Goldenberg, S. B., Landsea, C. W., Mestas-Nuñez, A. M., & Gray, W. M. (2001). The

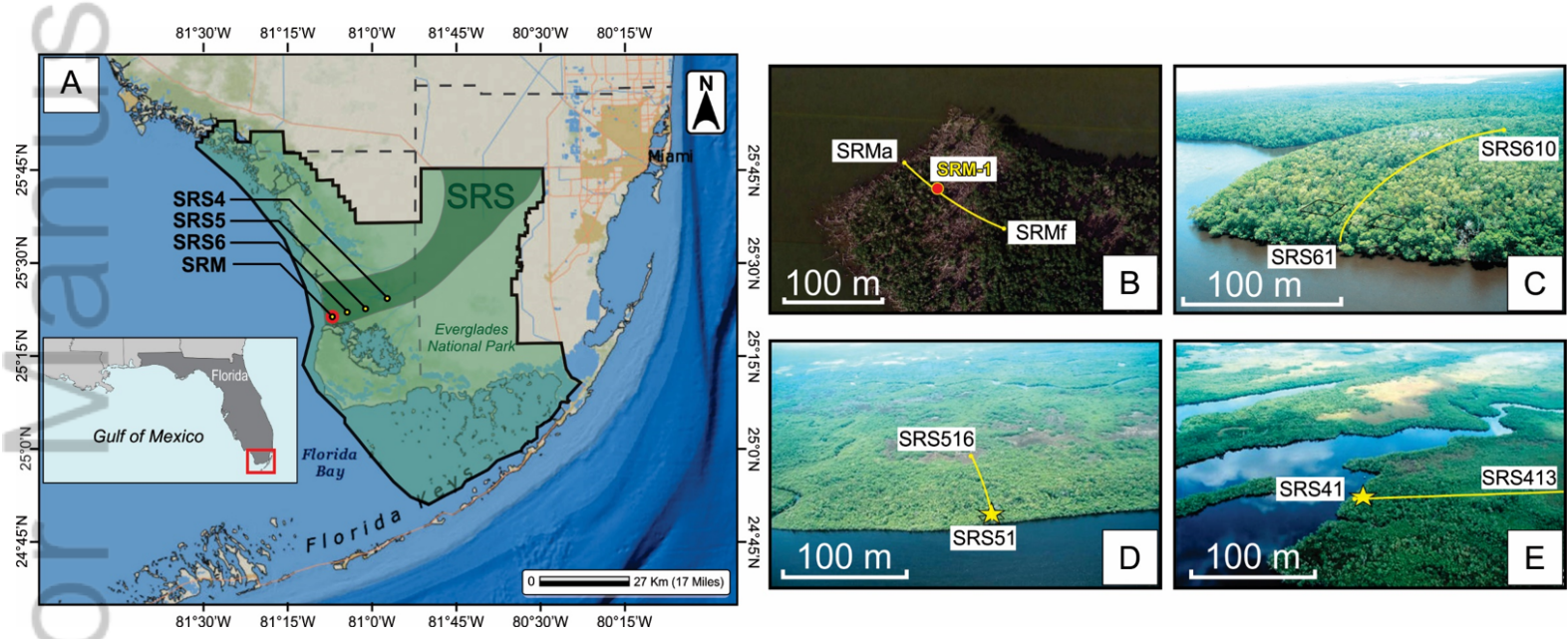
- 904 recent increase in Atlantic hurricane activity: Causes and
905 implications. *Science*, 293(5529), 474-479.
- 906 Haug, G. H., Hughen, K. A., Sigman, D. M., Peterson, L. C., & Röhl, U. (2001).
907 Southward migration of the intertropical convergence zone through the
908 Holocene. *Science*, 293(5533), 1304-1308.
- 909 van Hengstum, P. J., Donnelly, J. P., Toomey, M. R., Albury, N. A., Lane, P., &
910 Kakuk, B. (2014). Heightened hurricane activity on the Little Bahama Bank from
911 1350 to 1650 AD. *Continental Shelf Research*, 86, 103–115.
- 912 Hodell, D. A., Curtis, J. H., Jones, G. A., Higuera-Gundy, A., Brenner, M., Binford,
913 M. W., & Dorsey, K. T. (1991). Reconstruction of Caribbean climate change
914 over the past 10, 500 years. *Nature*, 352(6338), 790–793.
- 915 Houston, S. H., & Powell, M. D. (2003). Surface Wind Fields for Florida Bay
916 Hurricanes. *Journal of Coastal Research*, 19(3), 503–513.
- 917 Lamb, A. L., Wilson, G. P., & Leng, M. J. (2006). A review of coastal palaeoclimate
918 and relative sea-level reconstructions using $\delta^{13}\text{C}$ and C/N ratios in organic
919 material. *Earth-Science Reviews*, 75(1–4), 29–57.
- 920 Lambert, J. W., Aharon, P., & Rodriguez, A. B. (2008). Catastrophic hurricane
921 history revealed by organic geochemical proxies in coastal lake sediments: a case
922 study of Lake Shelby, Alabama (USA). *Journal of Paleolimnology*, 39(1), 117–
923 131.
- 924 Landsea, C. W., Franklin, J. L., McAdie, C. J., Beven, J. L., Gross, J. M., Jarvinen, B.
925 R., et al. (2004). A Reanalysis of Hurricane Andrew's Intensity. *Bulletin of the*
926 *American Meteorological Society*, 85(11), 1699–1712.
- 927 Lane, C. S., Hildebrandt, B., Kennedy, L. M., LeBlanc, A., Liu, K.-B., Wagner, A. J.,
928 & Hawkes, A. D. (2017). Verification of tropical cyclone deposits with oxygen
929 isotope analyses of coeval ostracod valves. *Journal of Paleolimnology*, 57(3),
930 245–255.
- 931 Lane, P., Donnelly, J. P., Woodruff, J. D., & Hawkes, A. D. (2011). A decadal-
932 resolved paleohurricane record archived in the late Holocene sediments of a
933 Florida sinkhole. *Marine Ecology*, 287(1-4), 14–30.
- 934 LeBlanc, A. R., Kennedy, L. M., Liu, K.B., & Lane, C. S. (2017). Linking hurricane
935 landfalls, precipitation variability, fires, and vegetation response over the past
936 millennium from analysis of coastal lagoon sediments, southwestern Dominican
937 Republic. *Journal of Paleolimnology*, 58(2), 135–150.
- 938 Liu, K.B. (2004). Paleotempestology: Principles, methods and examples from Gulf
939 coast lake sediments. In R. J. Murnane & K.B. Liu (Eds.), *Hurricanes and*
940 *Typhoons: Past, Present and Future*. New York: Columbia University Press.
- 941 Liu, K.B. (2013). Paleotempestology. In S. A. Elias (Ed.), *The Encyclopedia of*
942 *Quaternary Science*, vol. 3 (pp. 209-221). Elsevier.
- 943 Liu, K.B., & Fearn, M. L. (1993). Lake-sediment record of late Holocene hurricane
944 activities from coastal Alabama. *Geology*, 21(9), 793–796.
- 945 Liu, K.B., & Fearn, M. L. (2000). Reconstruction of Prehistoric Landfall Frequencies
946 of Catastrophic Hurricanes in Northwestern Florida from Lake Sediment
947 Records. *Quaternary Research*, 54(2), 238–245.
- 948 Liu, K.B., Lu, H., & Shen, C. (2008). A 1200-year proxy record of hurricanes and
949 fires from the Gulf of Mexico coast: Testing the hypothesis of hurricane–fire
950 interactions. *Quaternary Research*, 69(1), 29–41.
- 951 Liu, K.B., McCloskey, T.A., Ortego, S. and Maiti, K., 2014. Sedimentary signature of
952 Hurricane Isaac in a Taxodium swamp on the western margin of Lake
953 Pontchartrain, Louisiana, USA. *Proceedings of the International Association of*

- 954 *Hydrological Sciences*, 367, pp.421-428
955 Lodge, T. E. (2016). *The Everglades handbook: understanding the ecosystem*. Crc
956 Press.
- 957 Mann, M. E., Woodruff, J. D., Donnelly, J. P., & Zhang, Z. (2009). Atlantic
958 hurricanes and climate over the past 1,500 years. *Nature*, 460(7257), 880–883.
- 959 Mayfield, M., Avila, L., & Rappaport, E. N. (1994). Atlantic Hurricane Season of
960 1992. *Monthly Weather Review*, 122(3), 517–538.
- 961 McCloskey, T. A., & Liu, K. B. (2012) a. A 7000 year record of paleohurricane
962 activity from a coastal wetland in Belize. *Holocene*, 23(2), 278–291.
- 963 McCloskey, T. A., & Liu, K. B. (2012) b. A sedimentary-based history of hurricane
964 strikes on the southern Caribbean coast of Nicaragua. *Quaternary Research*,
965 78(3), 454–464.
- 966 McCloskey, T. A., & Liu, K. B. (2013). Sedimentary History of Mangrove Cays in
967 Turneffe Islands, Belize: Evidence for Sudden Environmental Reversals. *Journal*
968 *of Coastal Research*, 29(4), 971–983.
- 969 McCloskey, T. A., Bianchette, T. A., & Liu, K. B. (2013). Track Patterns of
970 Landfalling and Coastal Tropical Cyclones in the Atlantic Basin, Their
971 Relationship with the North Atlantic Oscillation (NAO), and the Potential Effect
972 of Global Warming. *American Journal of Climate Change*, 2(3A), 212-22.
973 doi: [10.4236/ajcc.2013.23A002](https://doi.org/10.4236/ajcc.2013.23A002).
- 974 McCloskey, T. A., Bianchette, T. A., & Liu, K. B. (2015). Geological and
975 Sedimentological Evidence of a Large Tsunami Occurring~ 1100 Year BP from
976 a Small Coastal Lake along the Bay of La Paz in Baja *Journal of Marine*
977 *Science and*. Retrieved from <http://www.mdpi.com/2077-1312/3/4/1544/htm>
- 978 McCloskey, T. A., Smith, C. G., Liu, K. B., Marot, M., & Haller, C. (2018). How
979 Could a Freshwater Swamp Produce a Chemical Signature Characteristic of a
980 Saltmarsh? *ACS Earth and Space Chemistry*, 2(1), 9–20.
- 981 McCloskey, T. A., Smith, C. G., Liu, K. B., & Nelson, P. R. (2018). The Effects of
982 Tropical Cyclone-Generated Deposition on the Sustainability of the Pearl River
983 Marsh, Louisiana: The Importance of the Geologic Framework. *Frontiers in*
984 *Ecology and Evolution*, 6. <https://doi.org/10.3389/fevo.2018.00179>
- 985 Moy, C. M., Seltzer, G. O., Rodbell, D. T., & Anderson, D. M. (2002). Variability of
986 El Niño/Southern Oscillation activity at millennial timescales during the
987 Holocene epoch. *Nature*, 420(6912), 162–165.
- 988 Naquin, J. D., Liu, K. B., McCloskey, T. A., & Bianchette, T. A. (2014). Storm
989 deposition induced by hurricanes in a rapidly subsiding coastal zone. *Journal of*
990 *Coastal Research*, 70, 308–313.
- 991 NOAA. (2019). NOAA Historical Hurricane Tracks. Retrieved November 26, 2019,
992 from <https://oceanservice.noaa.gov/news/historical-hurricanes/>
- 993 Parkinson, R. W. (1989). Decelerating Holocene sea-level rise and its influence on
994 Southwest Florida coastal evolution; a transgressive/regressive stratigraphy.
995 *Journal of Sedimentary Research*, 59(6), 960–972.
- 996 Park, L. E. (2012). Comparing Two Long-Term Hurricane Frequency and Intensity
997 Records from San Salvador Island, Bahamas. *Journal of Coastal Research*, 891–
998 902.
- 999 Ramírez-Herrera, M.-T., Lagos, M., Hutchinson, I., Kostoglodov, V., Machain, M. L.,
1000 Caballero, M., et al. (2012). Extreme wave deposits on the Pacific coast of
1001 Mexico: Tsunamis or storms? — A multi-proxy approach. *Geomorphology* ,
1002 139-140, 360–371.
- 1003 Risi, J. A., Wanless, H. R., Tedesco, L. P., & Gelsanliter, S. (1995). Catastrophic

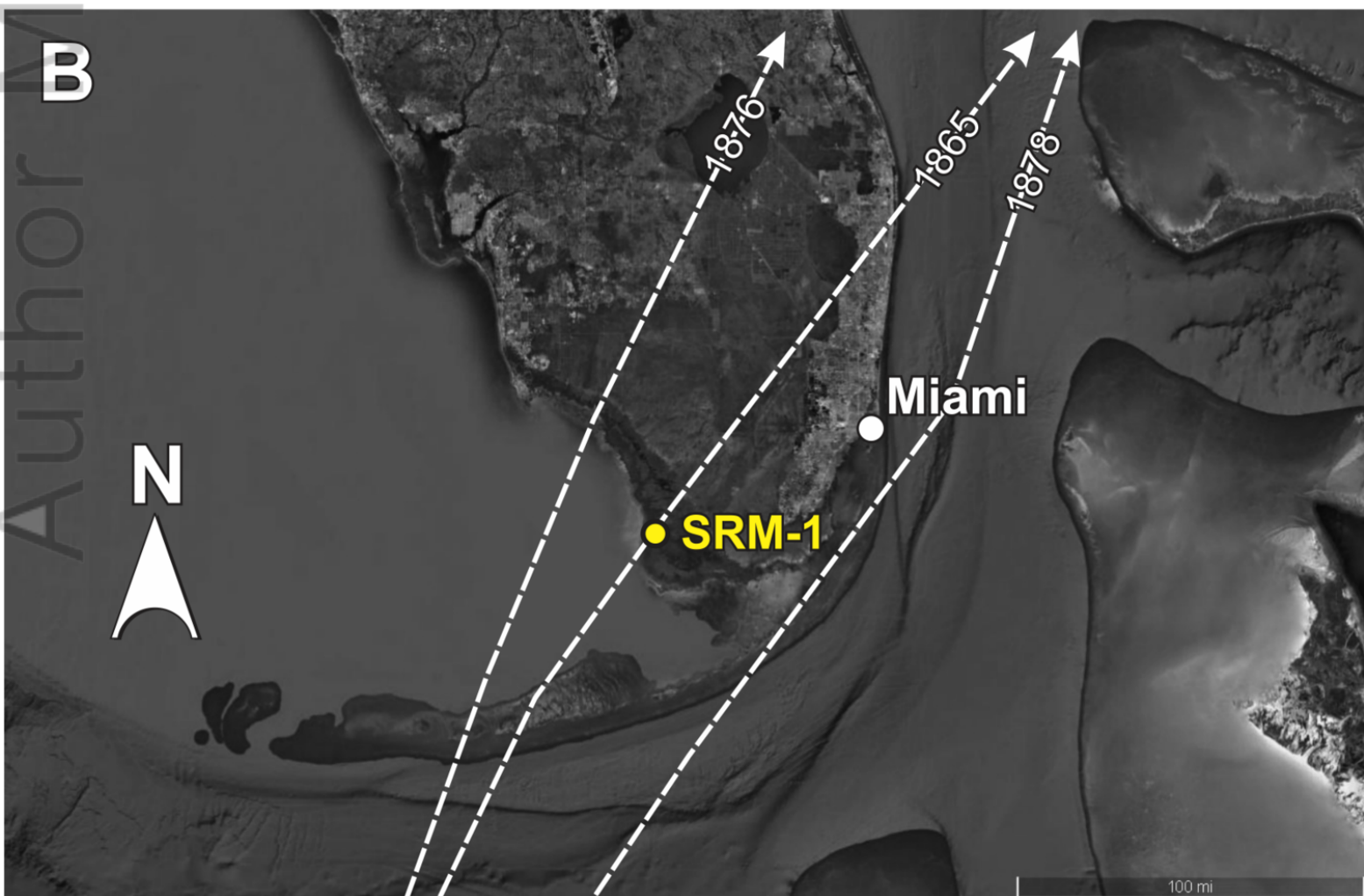
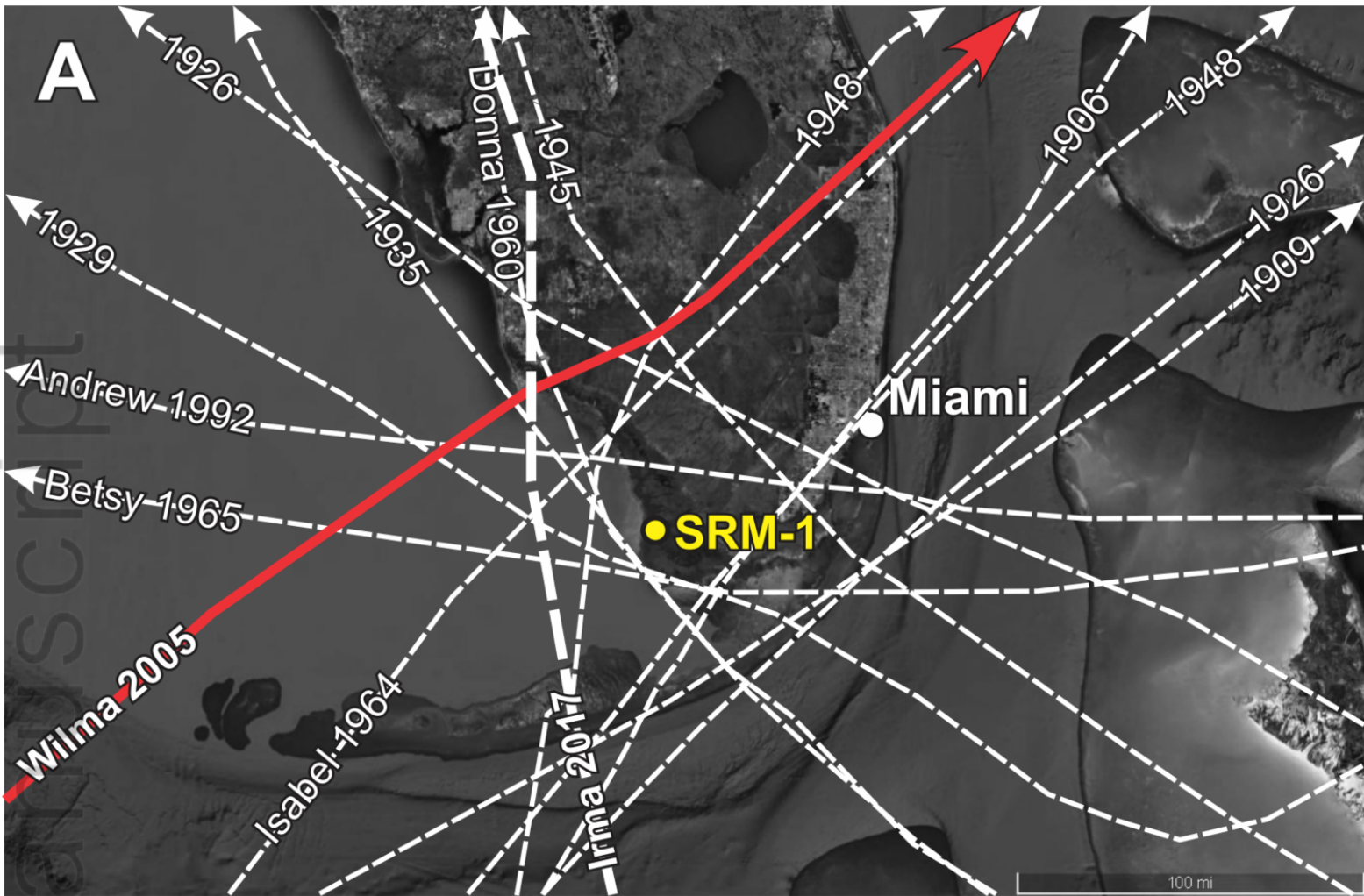
- 1004 Sedimentation from Hurricane Andrew Along the Southwest Florida Coast.
1005 *Journal of Coastal Research*, 83–102.
- 1006 Salkind, N. J. (2010). *Encyclopedia of research design* (Vol. 2). Sage.
- 1007 Scholl, D. W., Craighead, F. C., Sr, & Stuiver, M. (1969). Florida submergence curve
1008 revised: its relation to coastal sedimentation rates. *Science*, 163(3867), 562–564.
- 1009 Simard, M., Zhang, K., Rivera-Monroy, V. H., Ross, M. S., Ruiz, P. L., Castañeda-
1010 Moya, E., et al. (2006). Mapping Height and Biomass of Mangrove Forests in
1011 Everglades National Park with SRTM Elevation Data. *Photogrammetric*
1012 *Engineering & Remote Sensing*, 72(3), 299–311.
- 1013 Simpson, R. H., & Riehl, H. (1981). *The hurricane and its impact*. Louisiana State
1014 University Press.
- 1015 Smith, T. J., Anderson, G. H., Balentine, K., Tiling, G., Ward, G. A., & Whelan, K.
1016 R. T. (2009). Cumulative impacts of hurricanes on Florida mangrove
1017 ecosystems: Sediment deposition, storm surges and vegetation. *Wetlands*, 29(1),
1018 24.
- 1019 Smoak, J. M., Breithaupt, J. L., Smith, T. J., & Sanders, C. J. (2013). Sediment
1020 accretion and organic carbon burial relative to sea-level rise and storm events in
1021 two mangrove forests in Everglades National Park. *Catena*, 104, 58–66.
- 1022 Van Soelen, E. E., Brooks, G. R., Larson, R. A., Sinninghe Damsté, J. S., & Reichart,
1023 G. J. (2012). Mid-to late-Holocene coastal environmental changes in southwest
1024 Florida, USA. *Holocene*, 22(8), 929–938.
- 1025 Wallace, D. J., & Anderson, J. B. (2010). Evidence of similar probability of intense
1026 hurricane strikes for the Gulf of Mexico over the late Holocene. *Geology*, 38(6),
1027 511–514.
- 1028 Wallace, D. J., Woodruff, J. D., Anderson, J. B., & Donnelly, J. P. (2014).
1029 Palaeohurricane reconstructions from sedimentary archives along the Gulf of
1030 Mexico, Caribbean Sea and western North Atlantic Ocean margins. *Geological*
1031 *Society, London, Special Publications*, 388(1), 481–501.
- 1032 Wanless, H. R., Parkinson, R. W., & Tedesco, L. P. (1994). Sea level control on
1033 stability of Everglades wetlands. *Everglades: The Ecosystem and Its Restoration*.
1034 *St. Lucie Press, Delray Beach, FL, USA*, 199–223.
- 1035 Whelan, K. R. T., Smith, T. J., Anderson, G. H., & Ouellette, M. L. (2009). Hurricane
1036 Wilma's impact on overall soil elevation and zones within the soil profile in a
1037 mangrove forest. *Wetlands*, 29(1), 16.
- 1038 WHO (2020). World Health Organization, Tropical Cyclones. Retrieved March 26,
1039 2020, from https://www.who.int/health-topics/tropical-cyclones#tab=tab_1
- 1040 Williams, H., & Liu, K.-B. (2019). Contrasting Hurricane Ike washover sedimentation
1041 and Hurricane Harvey flood sedimentation in a Southeastern Texas coastal
1042 marsh. *Marine Geology*, 417, 106011.
- 1043 Woodruff, J. D., Donnelly, J. P., Mohrig, D., & Geyer, W. R. (2008). Reconstructing
1044 relative flooding intensities responsible for hurricane-induced deposits from
1045 Laguna Playa Grande, Vieques, Puerto Rico. *Geology*, 36(5), 391–394.
- 1046 Woodruff, J. D., Donnelly, J. P., & Okusu, A. (2009). Exploring typhoon variability
1047 over the mid-to-late Holocene: evidence of extreme coastal flooding from
1048 Kamikoshiki, Japan. *Quaternary Science Reviews*, 28(17), 1774–1785.
- 1049 Yao, Q., & Liu, K. B. (2017). Dynamics of marsh-mangrove ecotone since the mid-
1050 Holocene: A palynological study of mangrove encroachment and sea level rise in
1051 the Shark River Estuary, Florida. *PLoS One*, 12(3), e0173670.
- 1052 Yao, Q., & Liu, K. B. (2018). Changes in Modern Pollen Assemblages and Soil
1053 Geochemistry along Coastal Environmental Gradients in the Everglades of South

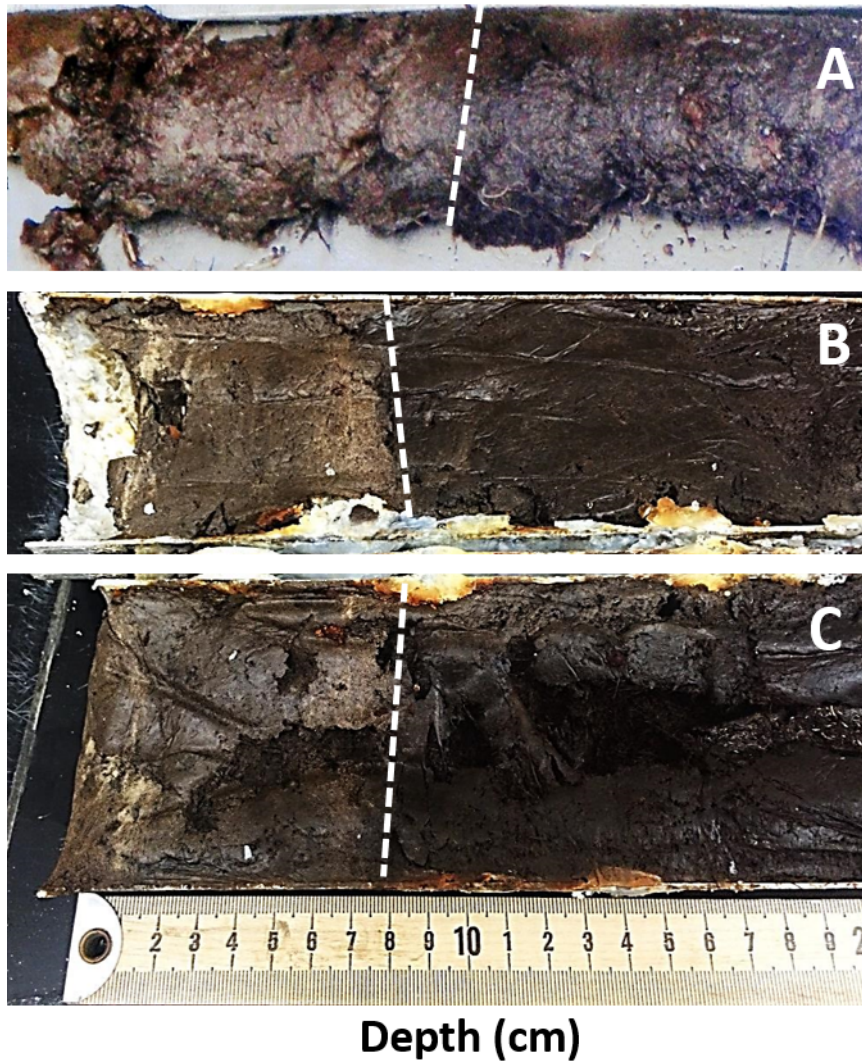
- 1054 Florida. *Frontiers in Ecology and Evolution*, 5, 178.
- 1055 Yao, Q., Liu, K. B., Platt, W. J., & Rivera-Monroy, V. H. (2015). Palynological
1056 reconstruction of environmental changes in coastal wetlands of the Florida
1057 Everglades since the mid-Holocene. *Quaternary Research*, 83(3), 449–458.
- 1058 Yao, Q., Liu, K. B., & Ryu, J. (2018). Multi-proxy Characterization of Hurricanes
1059 Rita and Ike Storm Deposits in the Rockefeller Wildlife Refuge, Southwestern
1060 Louisiana. *Journal of Coastal Research*, 85(SI), 841–845.
- 1061 Yao, Q., Liu, K. B., Williams, H., Joshi, S., Bianchette, T. A., Ryu, J., & Dietz, M.
1062 (2019). Hurricane Harvey Storm Sedimentation in the San Bernard National
1063 Wildlife Refuge, Texas: Fluvial Versus Storm Surge Deposition. *Estuaries and*
1064 *Coasts*. <https://doi.org/10.1007/s12237-019-00639-6>
- 1065 Zhang, K., Simard, M., Ross, M., Rivera-Monroy, V. H., Houle, P., Ruiz, P., et al.
1066 (2008). Airborne Laser Scanning Quantification of Disturbances from
1067 Hurricanes and Lightning Strikes to Mangrove Forests in Everglades National
1068 Park, USA. *Sensors*, 8(4), 2262–2292.
- 1069 Zhou, L., Gao, S., Yang, Y., Zhao, Y., Han, Z., Li, G., et al. (2017). Typhoon events
1070 recorded in coastal lagoon deposits, southeastern Hainan Island. *Acta*
1071 *Oceanologica Sinica*, 36(4), 37–45.
- 1072 Zhou, L., Yang, Y., Wang, Z., Jia, J., Mao, L., Li, Z., et al. (2019). Investigating
1073 ENSO and WPWP modulated typhoon variability in the South China Sea during
1074 the mid--late Holocene using sedimentological evidence from southeastern
1075 Hainan Island, China. *Marine Geology*, 416, 105987.

1076

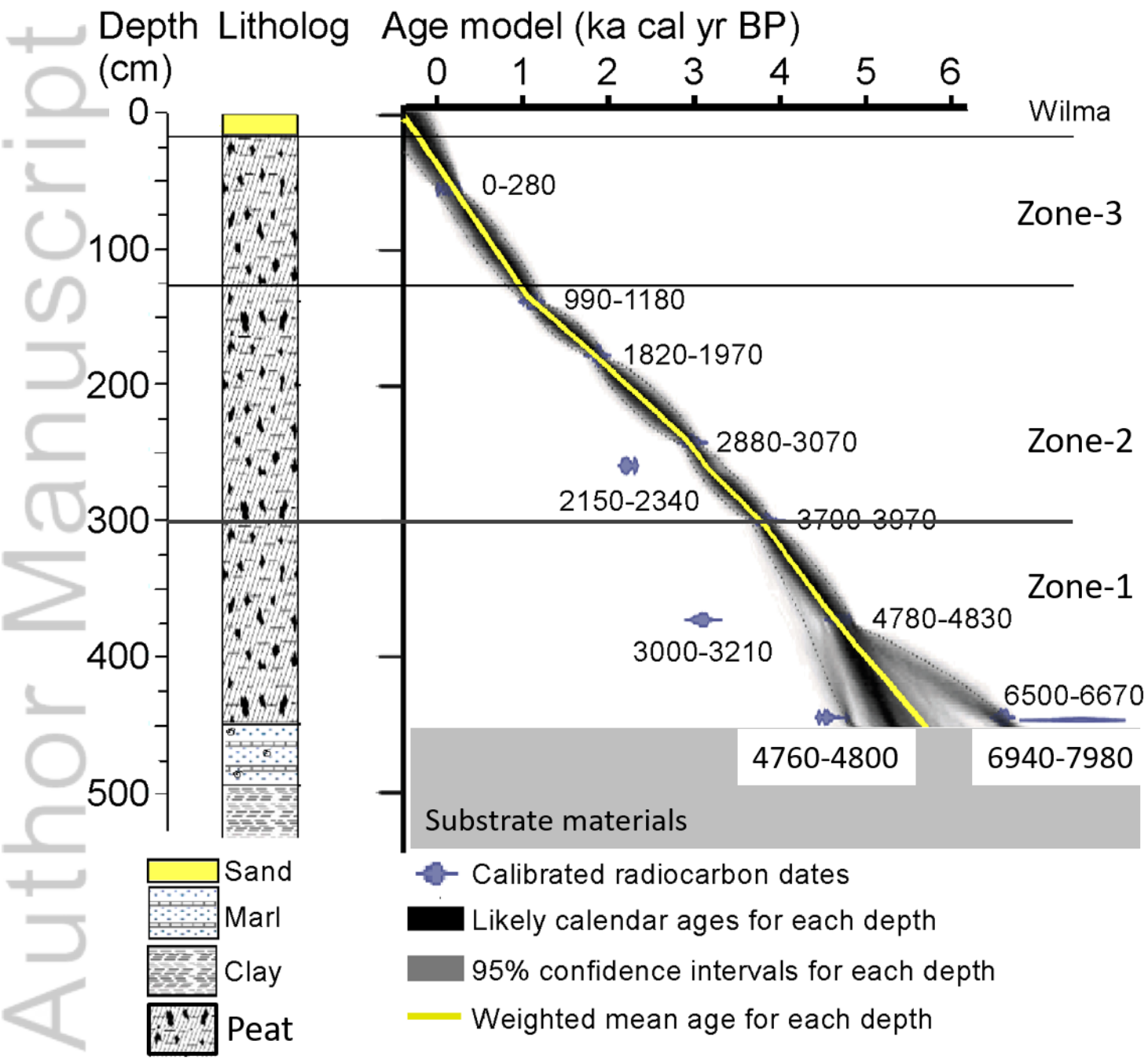


2019WR026857-f01-z-.tif

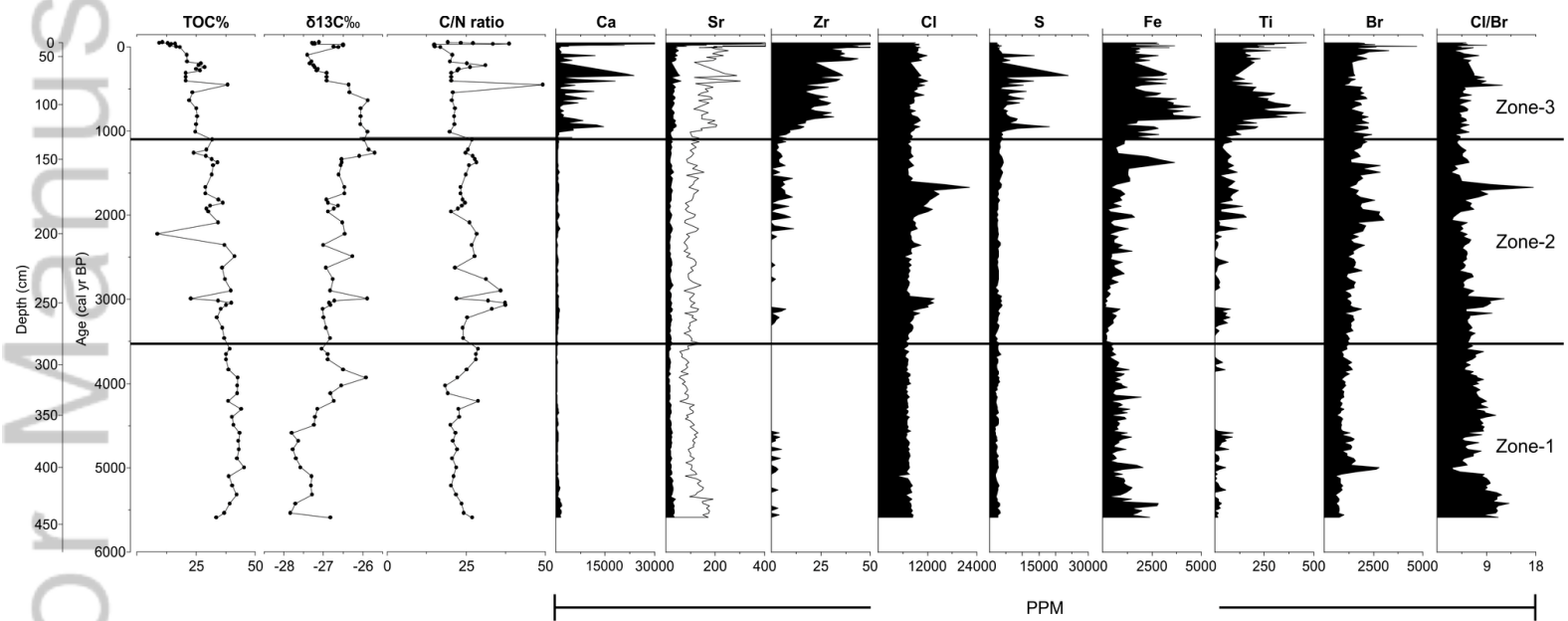




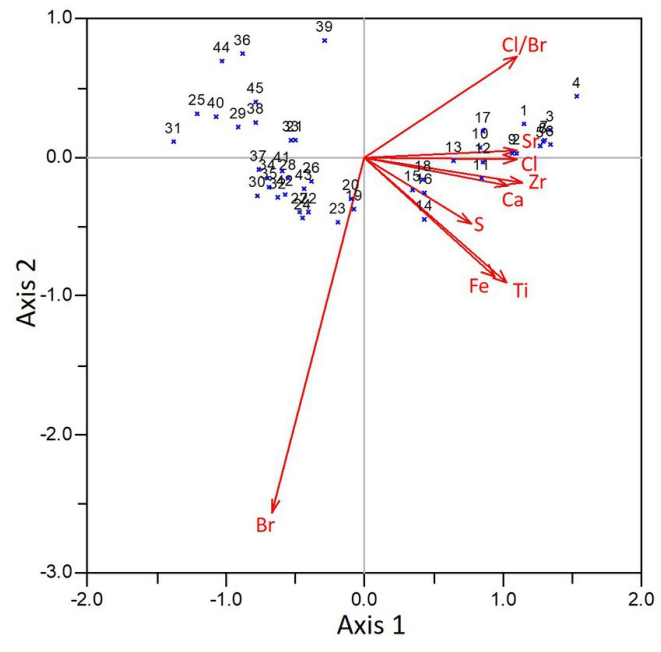
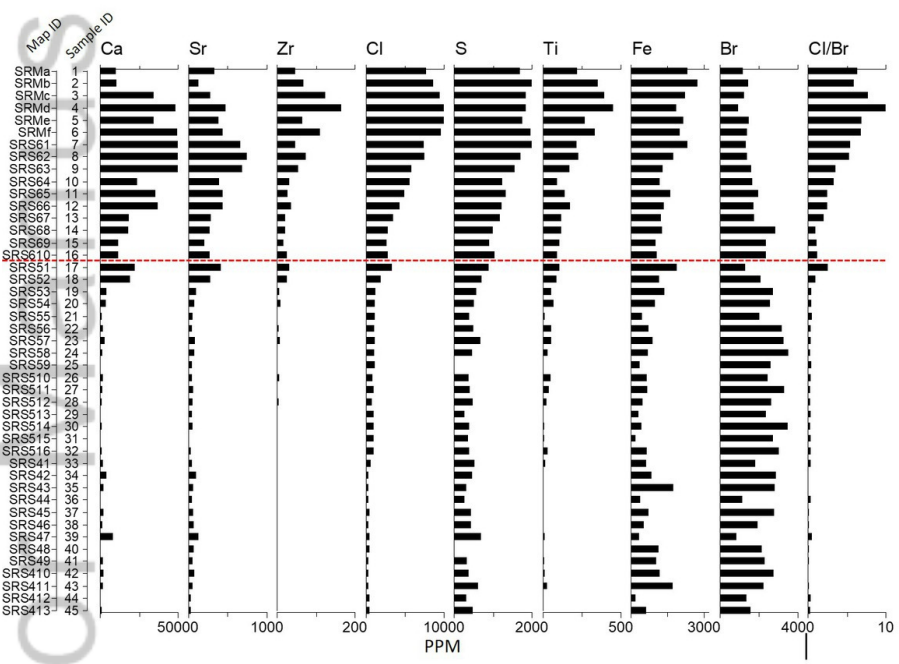
2019WR026857-f03-z.tif



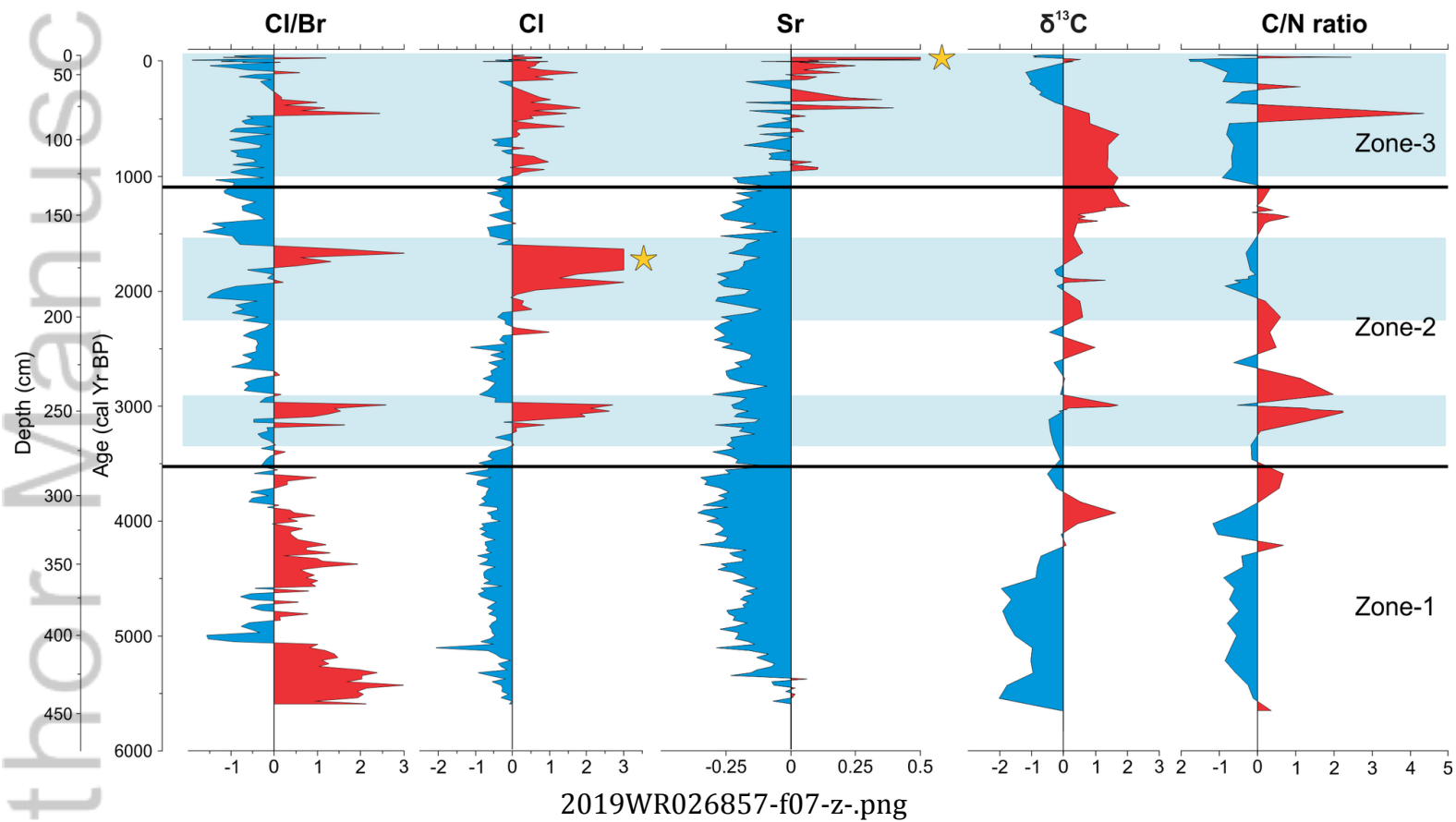
2019WR026857-f04-z.tif

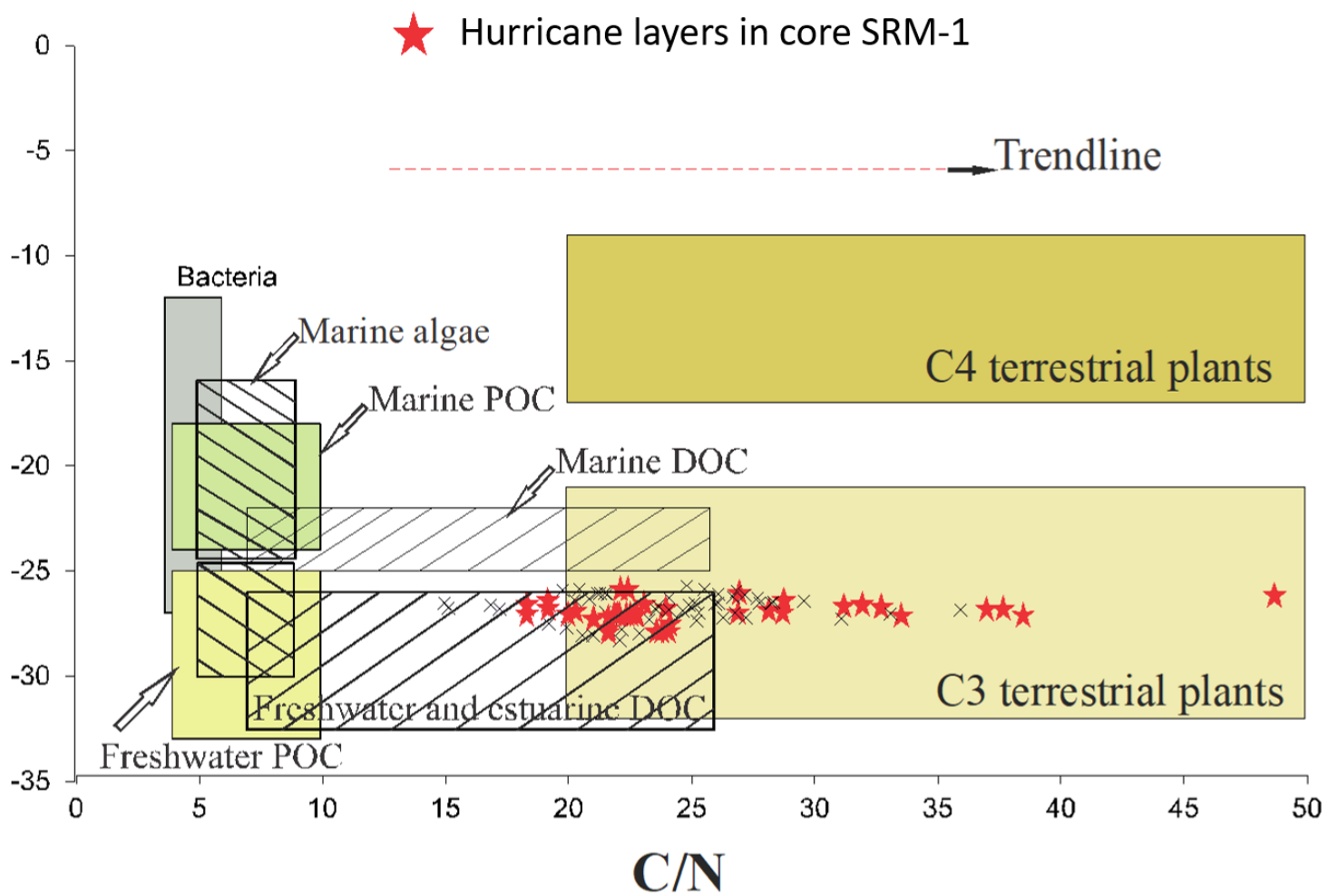


2019WR026857-f05-z-.png

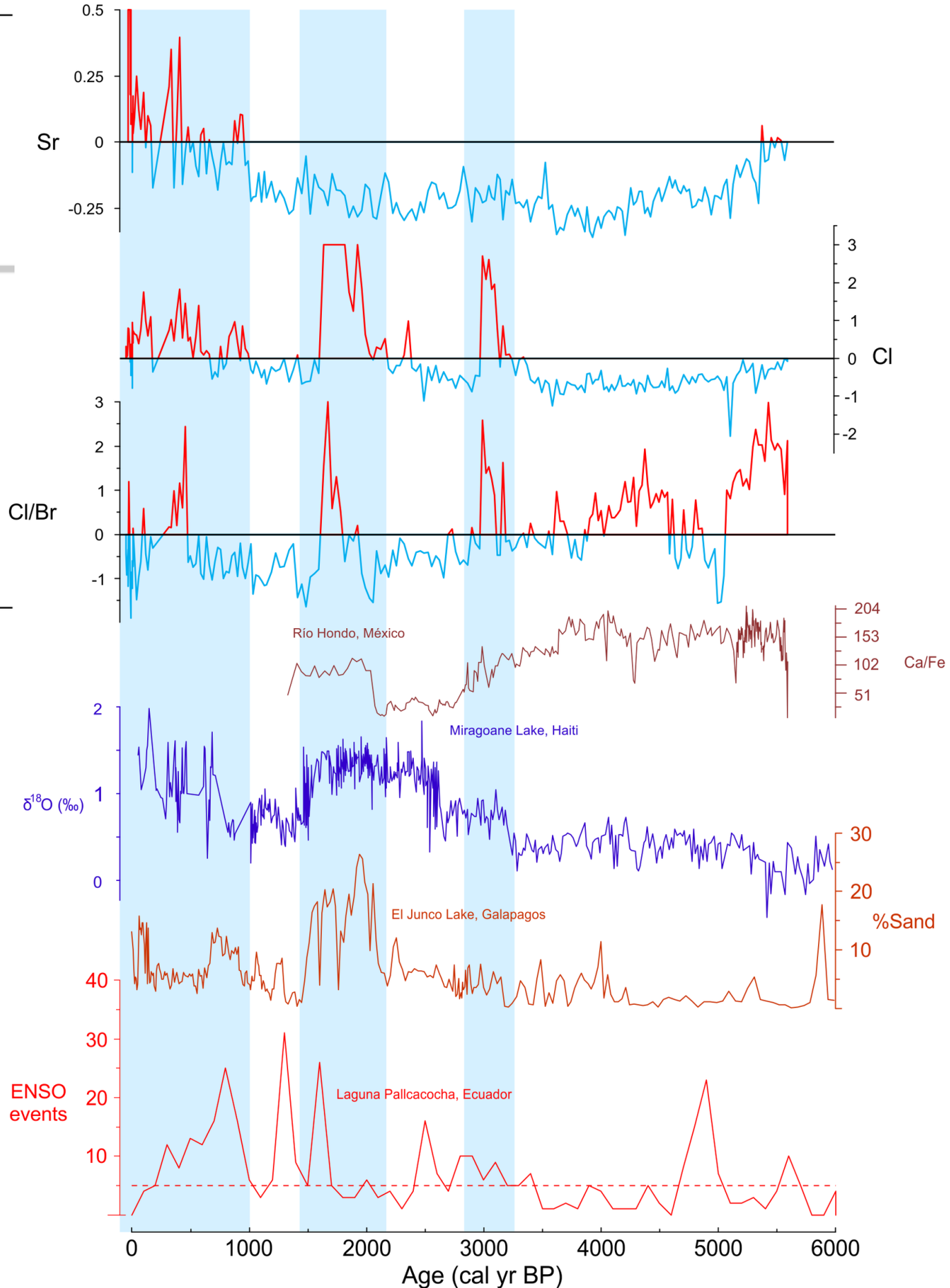


2019WR026857-f06-z-.jpg





2019WR026857-f08-z.tif



2019WR026857-f09-z-.png